AD-A035 050 ARMY MISSILE RESEARCH DEVELOPMENT AND ENGINEERING LAB--ETC F/G 17/9
QUASI-COHERENT DETECTOR PERFORMANCE WITH APPLICATION TO CW RADA--ETC(U)
OCT 76 T H GEE, R R BOOTHE

UNCLASSIFIED RE-77-1 NL

| OF |
AD
A035050

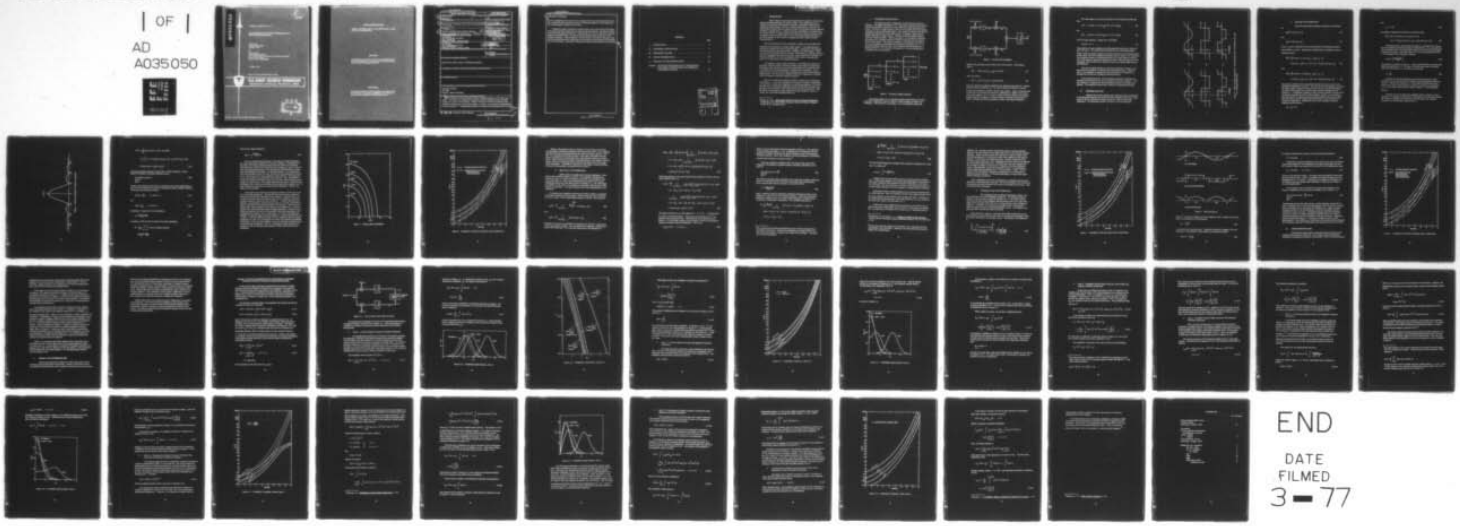

END

DATE
FILMED
3-77

TECHNICAL REPORT RE-77-1

QUASI-COHERENT DETECTOR PERFORMANCE WITH APPLICATION TO CW RADAR

Thomas H. Gee
Virginia Military Institute
Lexington, Virginia

and

Robert R. Boothe
Advanced Sensors Directorate
US Army Missile Research, Development and Engineering Laboratory
US Army Missile Command
Redstone Arsenal, Alabama 35809

1 October 1976

U.S. ARMY MISSILE COMMAND
Redstone Arsenal, Alabama 35809

DISPOSITION INSTRUCTIONS

DESTROY THIS REPORT WHEN IT IS NO LONGER NEEDED. DO NOT RETURN IT TO THE ORIGINATOR.

DISCLAIMER

THE FINDINGS IN THIS REPORT ARE NOT TO BE CONSTRUED AS AN OFFICIAL DEPARTMENT OF THE ARMY POSITION UNLESS SO DESIGNATED BY OTHER AUTHORIZED DOCUMENTS.

TRADE NAMES

USE OF TRADE NAMES OR MANUFACTURERS IN THIS REPORT DOES NOT CONSTITUTE AN OFFICIAL INDORSEMENT OR APPROVAL OF THE USE OF SUCH COMMERCIAL HARDWARE OR SOFTWARE.

UNCLASSIFIED

SECURITY CLASSIFICATION OF THIS PAGE *(When Data Entered)*

REPORT DOCUMENTATION PAGE

READ INSTRUCTIONS BEFORE COMPLETING FORM

1. REPORT NUMBER: RE-77-1	2. GOVT ACCESSION NO.
3. RECIPIENT'S CATALOG NUMBER	
4. TITLE *(and Subtitle)*: Quasi-Coherent Detector Performance with Application to CW Radar.	5. TYPE OF REPORT & PERIOD COVERED: Technical Report
	6. PERFORMING ORG. REPORT NUMBER: RE-77-1
7. AUTHOR(s): Thomas H. Gee, Virginia Military Institute Robert R. Boothe, Adv. Sensors Dir., MICOM	8. CONTRACT OR GRANT NUMBER(s): AMCMS Code 632303.11.21401 DA 1W362303A214 Element Code 6.23.03.A
9. PERFORMING ORGANIZATION NAME AND ADDRESS: Commander US Army Missile Command Attn: DRSMI-RE Redstone Arsenal, Alabama 35809	10. PROGRAM ELEMENT, PROJECT, TASK AREA & WORK UNIT NUMBERS 51 p.
11. CONTROLLING OFFICE NAME AND ADDRESS: Commander US Army Missile Command Attn: DRSMI-RPR Redstone Arsenal, Alabama 35809	12. REPORT DATE: 1 Oct 1976 13. NUMBER OF PAGES: 50
14. MONITORING AGENCY NAME & ADDRESS *(if different from Controlling Office)*	15. SECURITY CLASS. *(of this report)*: Unclassified 15a. DECLASSIFICATION/DOWNGRADING SCHEDULE

16. DISTRIBUTION STATEMENT *(of this Report)*

Approved for public release; distribution unlimited.

17. DISTRIBUTION STATEMENT *(of the abstract entered in Block 20, if different from Report)*

18. SUPPLEMENTARY NOTES

19. KEY WORDS *(Continue on reverse side if necessary and identify by block number)*

Coherent processor
CW radar
Doppler – phase processing

20. ABSTRACT *(Continue on reverse side if necessary and identify by block number)*

The evolution of a quasi-coherent detector having application to CW radar is presented. The detector is configured as parallel correlator channels which use digital techniques to process video signals. Doppler frequency channels and channels representing the initial phase of the received signal, or return, are employed to approximate a coherent detector. A distinguishing feature of the quasi-coherent detector lies in the

→ over

DD FORM 1 JAN 73 1473 EDITION OF 1 NOV 65 IS OBSOLETE

UNCLASSIFIED

SECURITY CLASSIFICATION OF THIS PAGE *(When Data Entered)*

403 086

ABSTRACT (Concluded)

use of a rectangular pulse train as the local signal which is correlated with the return. The rectangular pulse structure provides computational efficiency, while being optimized with respect to signal-to-noise ratio.

Analytical results of particular interest pertain to the comparative performance of the quasi-coherent detector and the optimum coherent detector, the latter providing a detection performance benchmark. In the absence of errors in estimation of doppler frequency and initial phase, it is shown that the detector performs about 0.35 dB inferior to optimum. With limitations of a finite number of processor channels, tradeoffs between implementation complexity and performance in the presence of estimation errors are discussed. Criteria for design of the quasi-coherent detector are presented.

CONTENTS

I. INTRODUCTION

Radar returns are generally characterized as signals which possess doppler dependent frequency and unknown phase. Such signals can be non-coherently processed to yield optimum detection performance within the constraints of unknown phase. However, if these constraints are removed, the performance of such a system is inferior to that of a coherent processor wherein the phase is exactly known. A signal processor configuration is considered in this report which is an approximation to the optimum coherent processor in that it employs a number of phase "bins," one of which approximates the phase of the return signal. In this context, this signal processor might be termed "quasi-coherent."

The work reported here was undertaken in support of an on-going Army program for development of a "quiet" radar system.[1] The signal format of interest is a pseudo-noise (PN) coded CW signal. In particular, the analyses and results which are presented pertain to biphase, PN coded signals. Maximal length PN code sequences are assumed. Performance of a signal processor-detector configuration as referred to in this report is defined as a measure of detection probability for a given probability of false alarm, with signal-to-noise (S/N) ratio acting as a variable parameter.

Accounting for range, doppler and phase, a potentially large number of processor channels might be required to achieve near optimum performance. Objectives of this reported work include determination of the tradeoffs which are available between implementation complexity and performance. It is envisioned that many of the processor operations can be best accomplished by digital means. For this reason, attention is given to configuring a processor which is conducive to the use of digital techniques.

Evolvement of the quasi-coherent detector is outlined in the discussion which follows. A series of modifications to the basic correlator configuration as employed to process video signals are described and analyzed. It is shown that with some restrictions/modifications of the conventional correlator configuration can be effected to yield near optimum detector performance. Still, the ability is preserved to employ digital processing techniques which are simple, fast, and within the state-of-the-art.

---

[1] Boothe, R. et al., Quiet Radar/Missile Guidance Technical Assessment, Final Report, US Army Missile Command, Redstone Arsenal, Alabama, TR-RE-76-12, September 1975.

II. PROCESSOR CONFIGURATION

The signal processor configuration of interest here is shown in Figure 1. This figure illustrates L × M × N processor channels which perform correlation operations between the return signal and locally generated waveforms. There are L range channels, where L is the length of the PN sequence employed to code the transmitted signal. This number is determined in part by operational requirements of the radar system. In addition, there exist M doppler channels per range channel. Associated with each doppler channel, there are N phase channels. Given the number L, it is desired to determine the number M × N channels required to achieve a specified level of performance for the detector. The primary objectives of the analyses which follow are to assess detector performance as a function of the number, M × N, of processor channels and S/N ratio, and to determine the interdependence of values of M and N. It is desirable to minimize M × N while maintaining an acceptable level of performance.

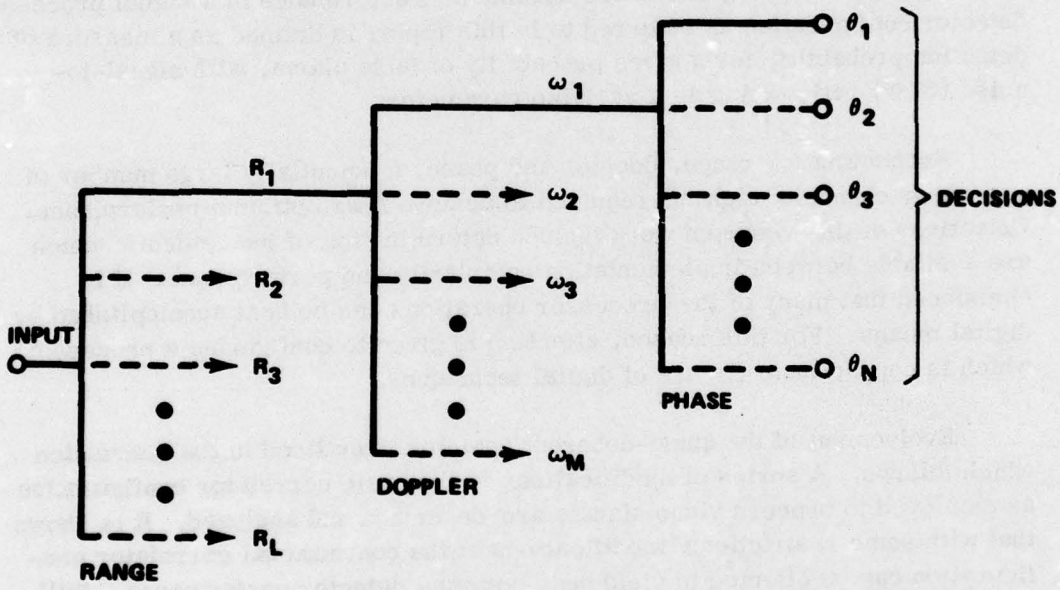

Figure 1. Processor channel structure.

Restricting attention to one particular doppler-phase channel, the video processor configuration shown in Figure 2 forms the basis for further consideration. With reference to this figure, a PN coded biphase signal with

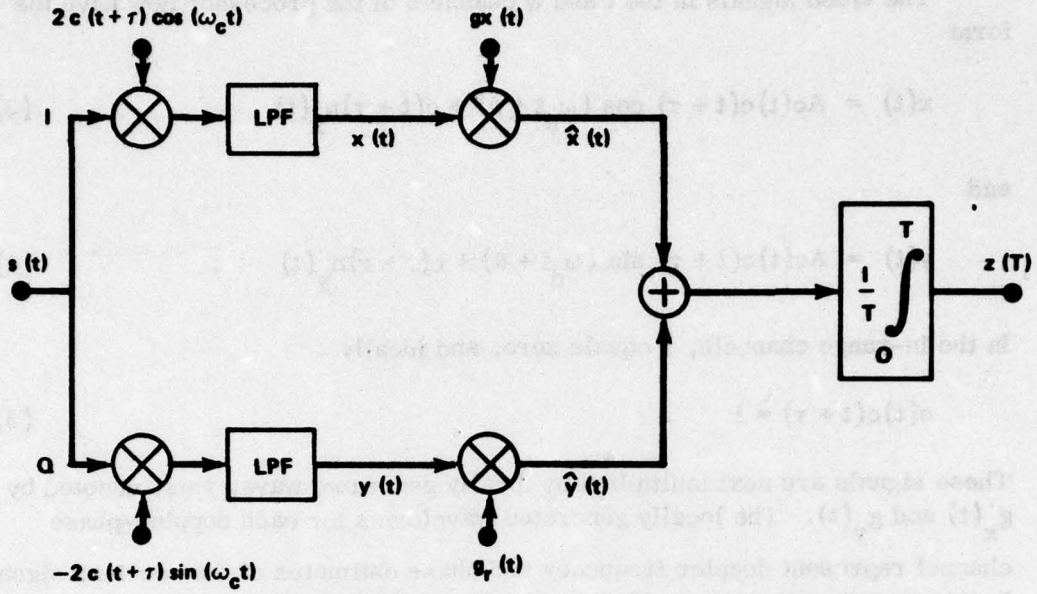

Figure 2. Processor block diagram.

additive white gaussian noise is input to the mixers shown. The received signal is

$$s(t) = Ac(t) \cos [(\omega_c + \omega_d)t + \theta] + n(t) \quad , \qquad (1)$$

where the noise is

$$n(t) = n_x(t) \cos (\omega_c t) - n_y(t) \sin (\omega_c t) \quad , \qquad (2)$$

and $c(t)$ represents a maximal length PN code sequence with values ±1. Doppler frequency shift is denoted by ω_d. The mixer outputs are filtered to produce in-phase and quadrature (I and Q) channel video signals. Figure 2 indicates that the PN code is removed at the mixers by multiplying by a shifted local replica of the code sequence, $c(t + \tau)$, where τ takes on discrete values corresponding to each range bin or channel. It is not necessary to decode at this point; but rather, decoding could be accomplished at video, using digital techniques.

The video signals in the I and Q channels of the processor now have the form

$$x(t) = Ac(t)c(t+\tau)\cos(\omega_d t + \theta) + c(t+\tau)n_x(t) \quad (3)$$

and

$$y(t) = Ac(t)c(t+\tau)\sin(\omega_d t + \theta) + c(t+\tau)n_y(t) \quad . \quad (4)$$

In the in-range channels, τ equals zero, and ideally

$$c(t)c(t+\tau) = 1 \quad . \quad (5)$$

These signals are next multiplied by locally generated waveforms, denoted by $g_x(t)$ and $g_y(t)$. The locally generated waveforms for each doppler-phase channel represent doppler frequency and phase estimates of the received signal. In this report, the three multiplier waveforms shown in Figure 3 are considered. The sinusoidal waveform is considered because it provides optimum performance if the frequency and phase estimates are exact, while the square wave and rectangular pulse waveform are conducive to the use of digital signal processing techniques.

The I and Q channel signals are summed as indicated by Figure 2, and then input to an integrator to complete the correlation process. Finally, at time T, the integrator is sampled and the sampled value is compared to a threshold for the purpose of making a detection decision.

In the following sections, results of analyses relevant to detector performance are presented for the three multiplier waveforms of Figure 3. Various methods of comparing the sampled integrator output to a threshold are possible. The appendix presents some of these for comparative purposes.

III. PROCESSOR ANALYSIS

Analysis of the quasi-coherent video signal processor is presented in the following paragraphs for each of the three multiplier waveforms. Equations (3) and (4) represent the signal input to the I and Q channel video multipliers. The sinusoidal waveform of Figure 3 is first considered.

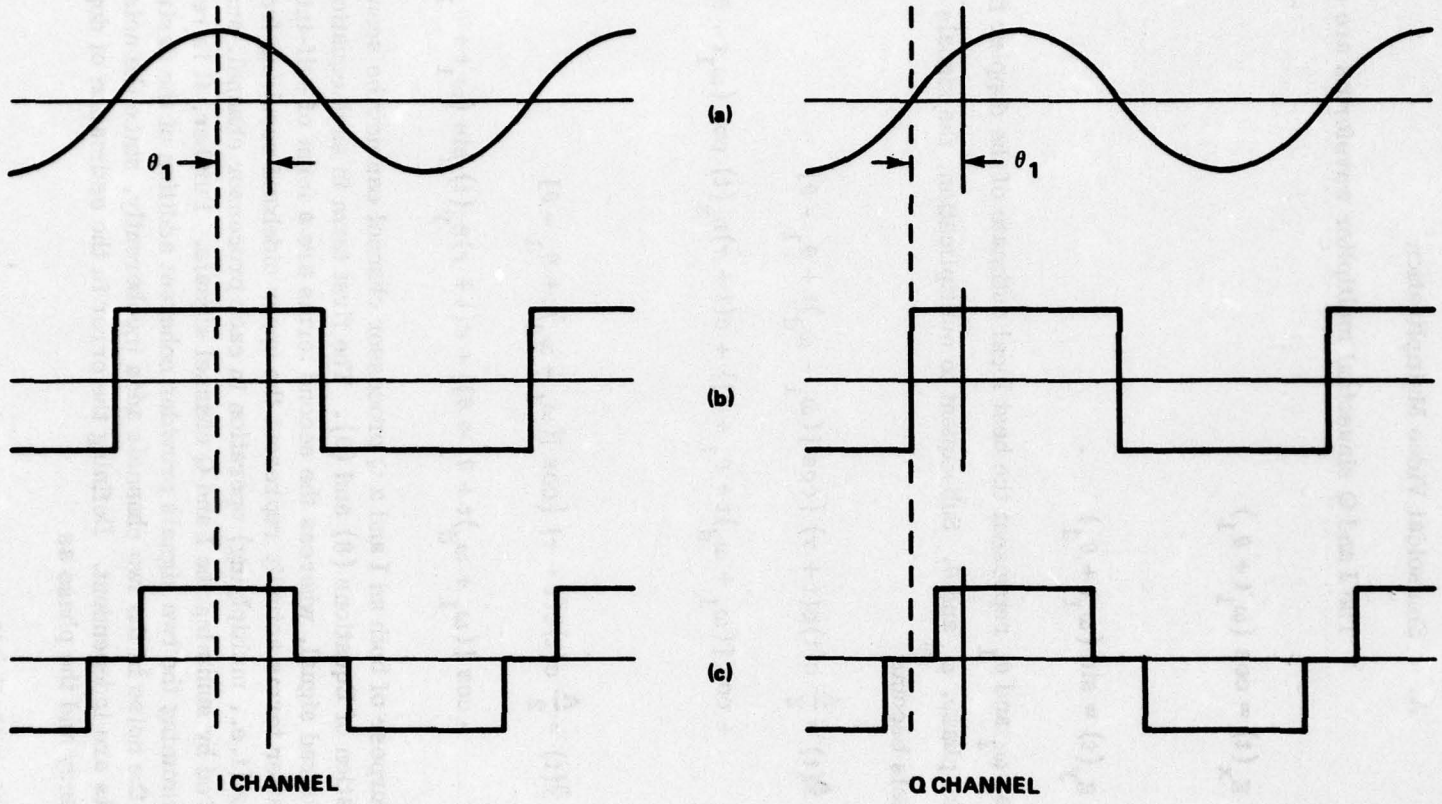

Figure 3. Video multiplier waveforms: (a) sinusoidal wave, (b) square wave, and (c) rectangular pulse train.

A. Sinusoidal Video Multiplication

The I and Q sinusoidal multiplier waveforms are expressed as

$$g_x(t) = \cos(\omega_1 t + \theta_1) \tag{6}$$

and

$$g_y(t) = \sin(\omega_1 t + \theta_1) \quad . \tag{7}$$

Above, ω_1 and θ_1 represent the best local estimate of the doppler frequency and the phase, ω_d and θ. Subsequent to multiplication, the signals in the two channels become

$$\hat{x}(t) = \frac{A}{2} c(t)c(t+\tau) \{\cos[(\omega_1 - \omega_d)t + \theta_1 - \theta] + \cos[(\omega_1 + \omega_d)t + \theta_1 + \theta]\} + c(t+\tau)n_x(t) \cos(\omega_1 t + \theta_1) \tag{8}$$

and

$$\hat{y}(t) = \frac{A}{2} c(t)c(t+\tau) \{\cos[(\omega_1 - \omega_d)t + \theta_1 - \theta] - \cos[(\omega_1 + \omega_d)t + \theta_1 + \theta]\} + c(t+\tau)n_y(t) \sin(\omega_1 t + \theta_1) \quad . \tag{9}$$

The purpose of both an I and a Q processor channel can now be seen by consideration of Equations (8) and (9). The first term in each equation represents the desired signal, whereas the second terms are a form of self-interference. The latter terms actually represent the upper sideband resulting from the mixing (i.e., multiplying) operation in each processor channel, and they can be removed by summing the I and Q channel signals. Further, it is recognized that summing the two signals provides coherent addition of the desired signal, while the noise in the two channels adds incoherently, since the noise components are independent. Defining the error in the estimation of doppler frequency and the phase as

$$\omega_1 - \omega_d = \Delta\omega \tag{10}$$

and

$$\theta_1 - \theta = \Delta\theta \quad , \tag{11}$$

the signals of Equations (8) and (9) are summed to give

$$\hat{x}(t) + \hat{y}(t) = Ac(t)c(t+\tau)\cos(\Delta\omega t + \Delta\theta)$$

$$+ c(t+\tau)\{n_x(t)\cos(\omega_1 t + \theta_1) + n_y(t)\sin(\omega_1 t + \theta_1)\} \quad . \tag{12}$$

Digressing briefly, the integrator of Figure 2 is considered for the purpose of presenting its frequency response characteristics. It is noted that this device integrates only over a finite time interval; or it performs the operation of integrate and dump. With a gain factor $1/T$, and an integration interval of T, the integrator has the frequency response

$$|H(f)| = \left| \frac{\sin(\pi f T)}{\pi f T} \right| \quad . \tag{13}$$

This function is sketched in Figure 4. It can be shown that the two-sided noise equivalent bandwidth is $1/T$. Further, with white input noise of two-sided power spectral density $\eta/2$, the output power becomes

$$N_0 = \frac{\eta}{2T} \quad . \tag{14}$$

Recalling the foregoing discussion concerning the presence of self-interference in the I and Q processor channels, the following observation can be made. With the aid of Figure 4, it is seen that this interference would appear at the output of the integrator, except in a case where the frequency $\omega_d + \omega_1$ has a period which is some integer multiple of T, the integration interval.

Returning now to the input of the integrator shown in Figure 2, and to Equation (12), attention is restricted to consideration of the in-range channels. The relation of Equation (5) is assumed, and this leads to the following expression for the integrator output at time T.

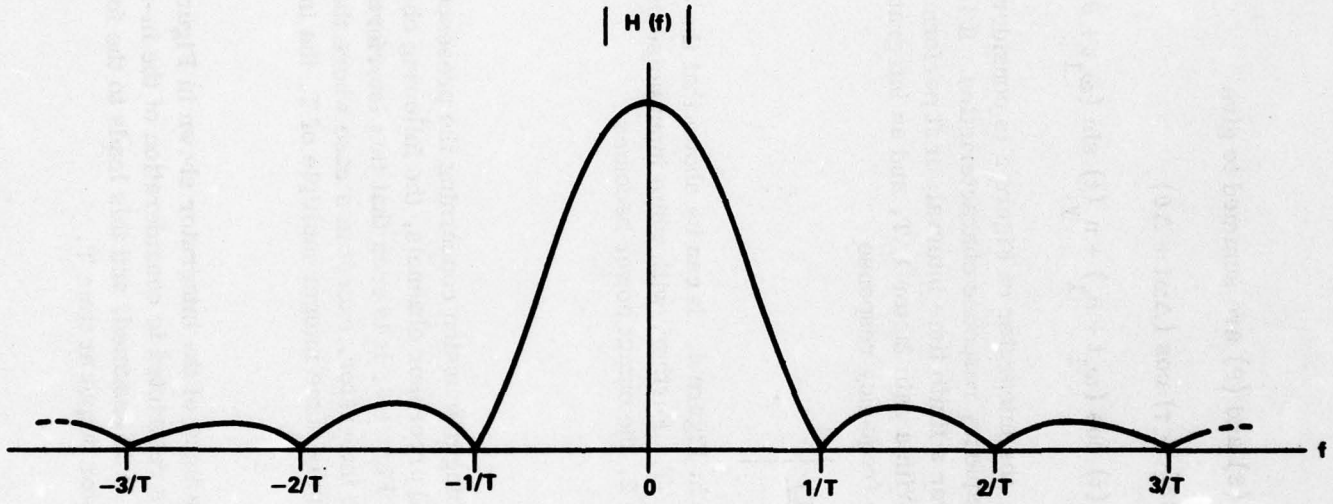

Figure 4. Sketch of integrator frequency response.

$$z(T) = \frac{A}{\Delta\omega T}\{\sin(\Delta\omega T + \Delta\theta) - \sin(\Delta\theta)\}$$

$$+ \frac{1}{T}\int_0^T c(t+\tau)\{n_x(t)\cos(\omega_1 t + \theta_1) + n_y(t)\sin(\omega_1 t + \theta_1)\}$$

$$= U(\Delta\omega T, \Delta\theta) + n_x(T) + n_y(T) \quad . \tag{15}$$

The desired signal component, $U(\Delta\omega T, \Delta\theta)$, is first considered. In the absence of frequency and phase estimation errors,

$$\lim_{\substack{\Delta\omega T \to 0 \\ \Delta\theta \to 0}} \{U(\Delta\omega T, \Delta\theta)\} = A \quad . \tag{16}$$

To gain some insight into the effects of estimation errors upon signal degradation, it is assumed that both errors are independent random variables uniformly distributed with probability densities

$$f(\Delta\omega T) = \frac{1}{2\beta} \quad , \quad -\beta \le \Delta\omega T \le \beta \tag{17}$$

and

$$f(\Delta\theta) = \frac{1}{2\alpha} \quad , \quad -\alpha \le \Delta\theta \le \alpha \quad . \tag{18}$$

Degradation in signal level is now defined by

$$D = \frac{U(\Delta\omega T, \Delta\theta)}{A} \quad . \tag{19}$$

Averaging on both $\Delta\omega T$ and $\Delta\theta$ gives the average degradation,

$$\bar{D} = \frac{1}{4\alpha\beta}\int_{-\beta}^{\beta}\int_{-\alpha}^{\alpha} U(\Delta\omega T, \Delta\theta)\, d(\Delta\theta)\, d(\Delta\omega T)$$

$$= \frac{\sin(\alpha)}{\alpha}\,\frac{\mathrm{Si}(\beta)}{\beta} \quad , \tag{20}$$

with the sine integral defined by

$$\mathrm{Si}(\xi) = \int_0^{\xi} \frac{\sin(t)}{t}\, dt \quad . \tag{21}$$

Prior to completing the discussion on the effects of signal degradation, the noise components in Equation (15) must be considered. Multiplication of the noise by the locally generated replica of the PN code acts to spread the noise spectrum, at best; and it leaves the noise unchanged, at worst. Which of these two possibilities actually occurs depends upon the bandwidth at the point where multiplication takes place. To avoid this question, it is assumed that after being multiplied by the PN code, the noise has two-sided spectral density of $\eta/2$, at the input to the video multipliers in each channel. This assumption can be made without loss of generality in the analyses. Next, multiplication by the unit amplitude sinusoidal waveforms in the video reduces the noise power density by a factor of two. (The signal suffers the same loss.) With reference to Equation (14), the total noise variance at the output of the integrator is $\eta/2T$ after summing the variances of the I and Q noise components. Further, the output noise is gaussian.

Data obtained from Equation (20) appears in Figure 5 in the form of contours of average degradation. Although this development does not guarantee that detector performance degradation obeys Figure 5, it has been shown via computer simulation that these data are valid at 50% probability of detection, and approximately so below this value (Figure 6). At higher detection probabilities, corresponding to relatively large values of S/N ratio, degradation in detector performance is greater than Figure 5 would imply. This is an interesting result, since Equation (20) was derived for an infinite S/N. However, Equation (20) gives the average value of signal degradation. If values of $\Delta\omega T$ and $\Delta\theta$ are selected from the set of permissible values corresponding to 1-dB degradation (for example, $\Delta\omega T = 1$ rad and $\Delta\theta = 0.6$ rad), it is found using Equation (15) that the signal component degrades 7.2 dB for this particular set of values. Such large values occur with very low probability when the average degradation is 1 dB. But, at the higher S/N ratios where detection probability exceeds 90%, only a very few detection misses are necessary to degrade detector performance significantly. That is, a significantly larger signal level is required in order to eliminate these detection misses which occur with low probability.

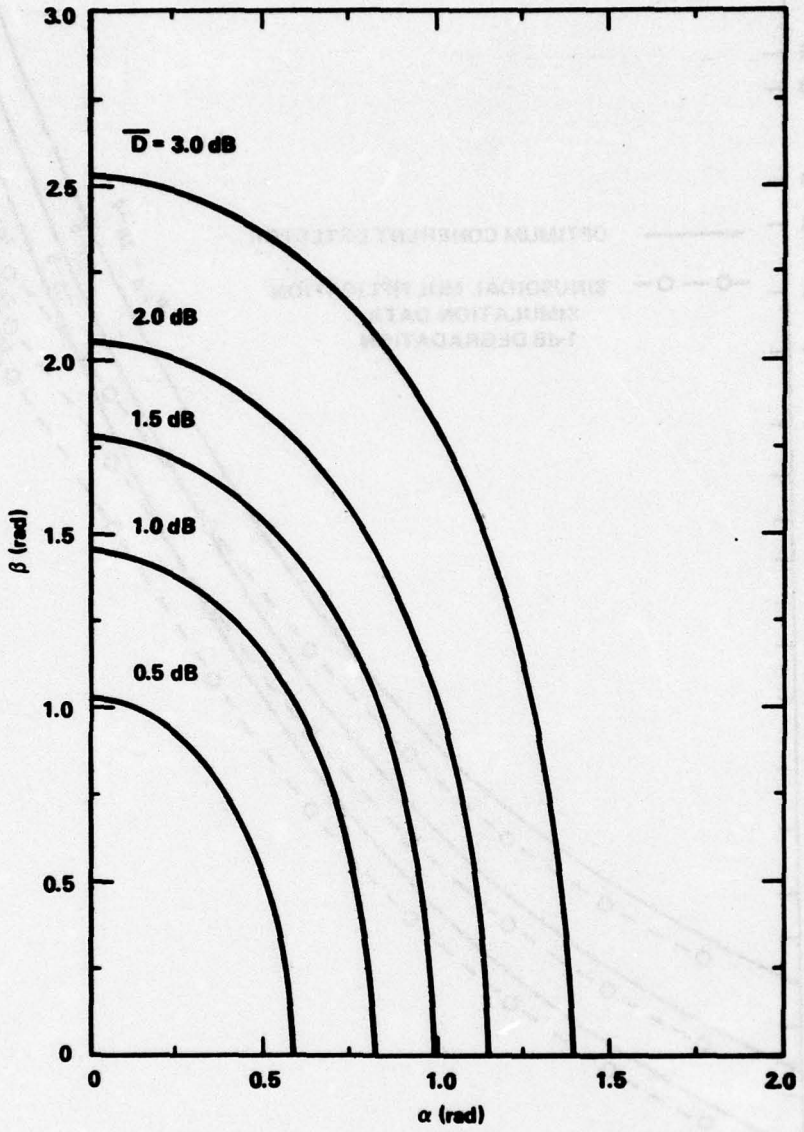

Figure 5. Average signal degradation.

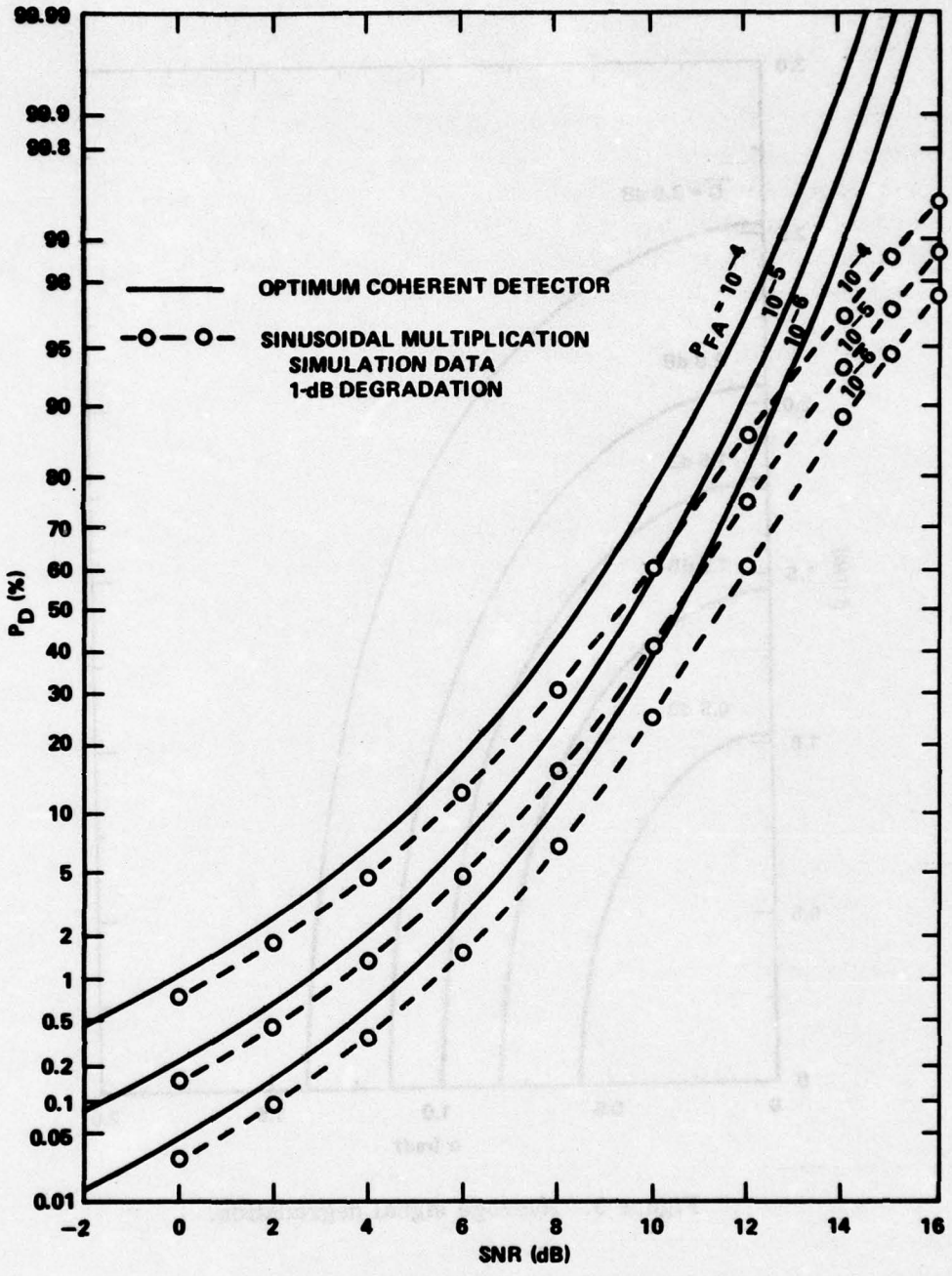

Figure 6. Probability of detection sinusoidal video multiplication.

Finally, with regards to the use of Figure 5 at low values of S/N ratio, corresponding to detection probability below approximately 10%, it is recognized that the noise plays an important part in the number of returns detected. Further, it is expected that the data of Figure 5 will reflect reasonably accurate detector performance on the average since many detection misses are encountered. Figure 6 permits comparison of the performance of an optimum coherent detector with that of the quasi-coherent detector operating with 1-dB average signal degradation. Probability of detection for the optimum coherent detector is derived in the appendix, and appears there as Case 1.

B. Square Wave Video Multiplication

Digital signal processing has its obvious advantages. If the quasi-coherent signal processor of Figure 2 were digitally implemented to process the video, it would be expedient to use square wave multiplier waveforms with values ±1. Such video multiplications are tantamount to simply changing the sign of the video signal when it is negative; i.e., the video signal is rectified, but the noise is not rectified (a step which would adversely affect detector performance). The effect of square wave video multiplication is now considered.

The square wave multiplier waveforms are shown in Figure 3 as applied in the I and Q channels of the processor. These waveforms can be expressed as Fourier series, with the appropriate phasing for I and Q. The series are

$$g_x(t) = \frac{4}{\pi} \sum_{n=1,3,5,\ldots} \frac{(-1)^{\frac{n-1}{2}}}{n} \cos(n\omega_1 t + n\theta_1) \tag{22}$$

and

$$g_y(t) = \frac{4}{\pi} \sum_{n=1,3,5,\ldots} \frac{1}{n} \sin(n\omega_1 t + n\theta_1) \quad . \tag{23}$$

Equations (3) and (4) are multiplied by Equations (22) and (23), respectively, to give the multiplier outputs. Upon summing the two channels, certain terms cancel while others add. The composite signal input to the integrator is

$$\hat{x}(t) + \hat{y}(t) = \frac{4A}{\pi} c(t)\, c(t+\tau) \Bigg\{ \sum_{n=1,5,9,\ldots} \frac{1}{n} \cos\left([(n-1)\omega_1 + \Delta\omega]t + (n-1)\theta_1 + \Delta\theta\right) - \sum_{n=3,7,11,\ldots} \frac{1}{n} \cos\left([(n+1)\omega_1 - \Delta\omega]t + (n+1)\theta_1 - \Delta\theta\right) \Bigg\} + c(t+\tau)\left\{g_x(t) n_x(t) \cos(\omega_1 t + \theta_1) + g_y(t) n_y(t) \sin(\omega_1 t + \theta_1)\right\} \quad . \tag{24}$$

Restricting attention to in-range channels where Equation (5) holds, the integrator output at time T is

$$z(T) = \frac{4A}{\pi} \sum_{n=1,5,9,\ldots} \frac{1}{n[(n-1)\omega_1 + \Delta\omega]T} \left\{\sin\left([(n-1)\omega_1 + \Delta\omega]T + (n-1)\theta_1 + \Delta\theta\right) - \sin[(n-1)\theta_1 + \Delta\theta]\right\}$$

$$- \sum_{n=3,7,11,\ldots} \frac{1}{n[(n+1)\omega_1 - \Delta\omega]T} \left\{\sin\left([(n+1)\omega_1 - \Delta\omega]T + (n+1)\theta_1 - \Delta\theta\right) - \sin[(n+1)\theta_1 - \Delta\theta]\right\} + n_x(T) + n_y(T)$$

$$= U(\Delta\omega T, \Delta\theta) + n_x(T) + n_y(T) \quad . \tag{25}$$

The higher harmonics of ω_1 which appear (i.e., 4, 8, 12, ...th harmonics) are a form of self-interference. The power in each reduces as $1/n^4$ as a function of the harmonic number. With reference to the sketch shown in Figure 4, it is noted that location of the harmonics at zeros of the integrator frequency response appears advantageous. That is, let

$$4\omega_m T = r2\pi \quad , \quad r = 1, 2, 3, \ldots \tag{26}$$

where m is one of the doppler channels appearing in Figure 1. (For purposes of the foregoing discussion, m = 1). If Equation (26) is satisfied for the 4th harmonic, all higher harmonics will also be located at zeros of the integrator frequency response. Under such conditions, the self-interference is minimized and that which remains is a function of $\Delta\omega T$.[2]

Under the conditions of Equation (26), the signal at the output of the integrator in the absence of doppler frequency and phase estimation error is given by

$$\lim_{\substack{\Delta\omega T \to 0 \\ \Delta\theta \to 0}} \{U(\Delta\omega T, \Delta\theta)\} = \frac{4A}{\pi} \quad . \tag{27}$$

The subject of average signal degradation due to frequency and phase estimation errors is of interest here as in the case of sinusoidal video multiplication. Here, using the same symbol as before to denote degradation,

$$D = \frac{U(\Delta\omega T, \Delta\theta)}{4A/\pi} \quad . \tag{28}$$

Again, assuming uniformly distributed probability densities for these errors, Equations (17) and (18) give the assumed densities. Following the approach indicated by Equation (20), the average signal degradation is obtained after considerable mathematical manipulation. The resulting expression is

$$\bar{D} = \frac{1}{2\beta} \frac{\sin(\alpha)}{\alpha} \sum_{n=1,5,9,\ldots} \frac{1}{n} \{\cos[(n-1)\theta_1][\mathrm{Si}[(n-1)\omega_1 T + \beta] - \mathrm{Si}[(n-1)\omega_1 T - \beta]] - \sin[(n-1)\theta_1][\mathrm{cin}[(n-1)\omega_1 T + \beta] - \mathrm{cin}[(n-1)\omega_1 T - \beta]]\}$$

---

[2] The so-called self-interference apparently occurs as either constructive or destructive interference. If these two possibilities are equally likely, then the restricting condition of Equation (26) might not be necessary. This point has not been investigated.

$$- \frac{1}{2\beta} \frac{\sin(\alpha)}{\alpha} \sum_{n=3,7,11,\ldots} \frac{1}{n} \{\cos[(n+1)\theta_1][\mathrm{Si}[(n+1)\omega_1 T + \beta]$$

$$- \mathrm{Si}[(n+1)\omega_1 T - \beta]] - \sin[(n+1)\theta_1][\mathrm{cin}[(n+1)\omega_1 T + \beta]$$

$$- \mathrm{cin}[(n+1)\omega_1 T - \beta]]\} \quad . \tag{29}$$

The sine integral appearing in Equation (29) is defined by Equation (21), while cin $(\cdot)$ is defined by[3]

$$\mathrm{cin}(\xi) = \int_0^{\xi} \frac{1 - \cos(t)}{t} \, dt \quad . \tag{30}$$

Equation (29) has been studied under the restriction given by Equation (26). Under such conditions, the average signal degradation is independent of the doppler frequency while dependence upon the initial phase is very small. It is, therefore, the case that Figure 5 provides a very good approximation of average signal degradation when the conditions of Equation (26) are satisfied.

Returning to further consider Equation (25), the noise components there are easily analyzed. Since the multiplier waveform has equally probable values of ±1, the presence of the multiplier does not affect the noise.[4] Denoting the two-sided noise spectral density in each video channel by $\eta/2$, the variance of the noise at the output of the integrator is η/T.

At this point, some insight into the performance of the detector using square wave video multiplication can be provided. In the absence of degradation, the signal given by Equation (27) is seen to be $4/\pi$ times that given by

---

[3] Abramowitz, M. and Stegun, I. A., Handbook of Mathematical Functions, National Bureau of Standards Applied Mathematics Series, Vol. 55, June 1964, p. 231.

[4] This is true only if the frequency of the square wave is less than twice the preintegrator video bandwidth. Otherwise, the noise spectrum is spread by square wave multiplication.

Equation (16), the latter actually representing optimum coherent detection. However, the noise variance in the square wave case is twice that for coherent detection. These numerical values show that the S/N ratio for square wave video multiplication is 0.9 dB below the same ratio obtained for the coherent detector. In the absence of estimation errors, computer simulation of the processor using square wave video multiplication confirms that 0.9-dB degradation in detection probability exists. Simulation data were also obtained with the processor operating in the presence of frequency and phase estimation errors. Representative results are presented in Figure 7 corresponding to 1-dB average signal degradation ($\Delta\theta = 0.6$ rad and $\Delta\omega T = 1$ rad). As predicted, at 50% probability of detection, performance is 1.9-dB inferior to optimum coherent detection. Pronounced deterioration is noted at the higher values of detection probability.

Next, rectangular pulse video multiplication is considered and compared with the two cases previously presented. Due to the similarity in the waveforms, the material previously presented can be used in presenting the next case. This is fortunate for all concerned.

C. Rectangular Pulse Video Multiplication

The rectangular pulse waveforms appearing in Figure 3 are now considered as the video multiplier waveforms. The significant characteristics of this waveform include the fact that it (i.e., the notch) removes noise from the input of the integrator during portions of the cycle of the video signal where the signal level is low (i.e., in the vicinity of zero crossings in Figure 8). In addition, the notch occurs such that it aids in reducing the effects of doppler frequency and phase estimation errors. The question to be addressed first concerns the width of the notch.

With reference to Figure 8, where the notch width is defined as 2ϕ rad, a first attempt to determine the notch width is to maximize the integrator output S/N ratio in the absence of estimation errors. The quantity to be maximized is

$$\frac{\left\{ A \int_{\phi}^{\pi/2} \sin(\omega t)\, d(\omega t) \right\}^2}{\sigma^2 \left(\frac{\pi - 2\phi}{\pi} \right)} = \frac{A^2 \cos^2(\phi)}{\sigma^2 \left(\frac{\pi - 2\phi}{\pi} \right)} , \qquad (31)$$

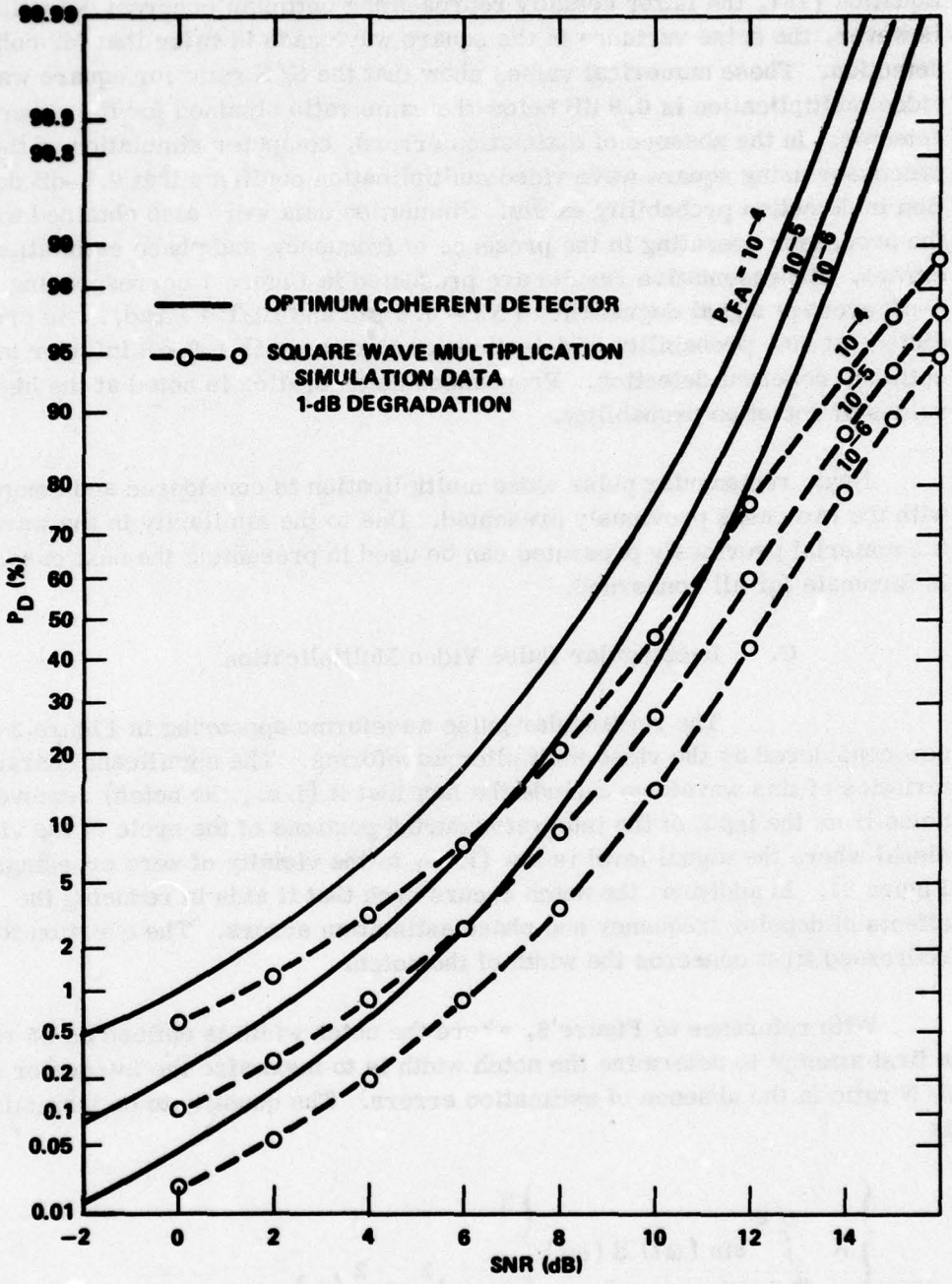

Figure 7. Probability of detection square wave multiplication.

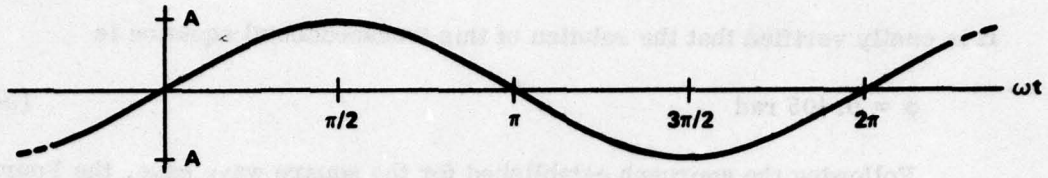

(a) VIDEO SIGNAL

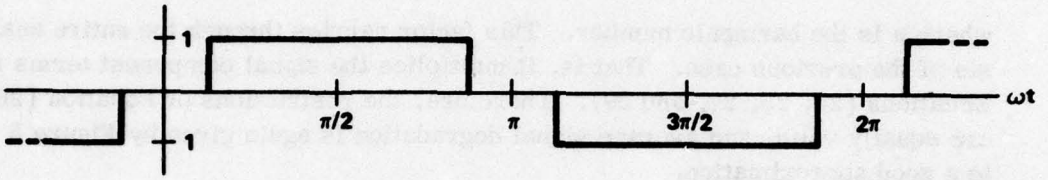

(b) MULTIPLIER WAVEFORM

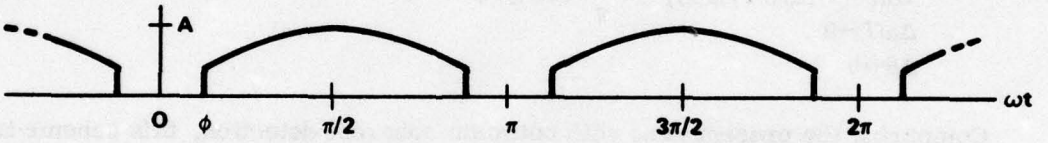

(c) MULTIPLIER OUTPUT

Figure 8. Video waveforms.

where σ^2 is the noise variance out of the integrator when ϕ equals zero, and the factor in parenthesis in the denominator,

$$R = \frac{\pi - 2\phi}{\pi} \tag{32}$$

is a noise power reduction factor. Taking the derivative of Equation (31) with respect to ϕ and setting the result equal to zero yields the relation

$$\tan(\phi) = \frac{1}{\pi - 2\phi} \quad . \tag{33}$$

It is easily verified that the solution of this transcendental equation is

$$\phi = 0.405 \text{ rad} \quad . \tag{34}$$

Following the approach established for the square wave case, the Fourier series representation for the rectangular pulse train (having values of 0 and ±1) is found to differ from Equations (22) and (23) by the multiplicative factor

$$C_n = \cos(n\phi) \quad , \quad n = 1, 3, 5, \ldots \tag{35}$$

where n is the harmonic number. This factor carries through the entire analysis of the previous case. That is, it multiplies the signal component terms in Equations (24, 25, 27, and 29). Therefore, the restrictions of Equation (26) are equally valid, and average signal degradation is again given by Figure 5 to a good approximation.

For the present case, the signal at the output of the integrator in the absence of estimation errors follows from Equation (27) to yield (n = 1)

$$\lim_{\substack{\Delta\omega T \to 0 \\ \Delta\theta \to 0}} \{U(\Delta\omega T, \Delta\theta)\} = \frac{4A}{\pi} \cos(\phi) \quad . \tag{36}$$

Comparing the present case with optimum coherent detection, this scheme is seen to be inferior by 0.35 dB when using Equation (34) and the noise reduction factor of Equation (32) in conjunction with Equation (36). Again, computer simulation confirms 0.35-dB degradation in detection probability when the estimation errors do not exist. Introducing frequency and phase estimation errors, the results of computer simulation show that Figure 5 is useful in predicting performance at 50% probability of detection and below. Illustrative data are presented by Figure 9. Comparison of Figures 6 and 9 reveals approximately 0.35-dB difference in performance also exists between sinusoidal and rectangular pulse video multiplication when estimation errors are present.

IV. DESIGN CONSIDERATIONS

Performance characteristics of the quasi-coherent detector were presented and assessed in Section III. Here design related considerations arising from the analytical treatment are presented. In view of the performance

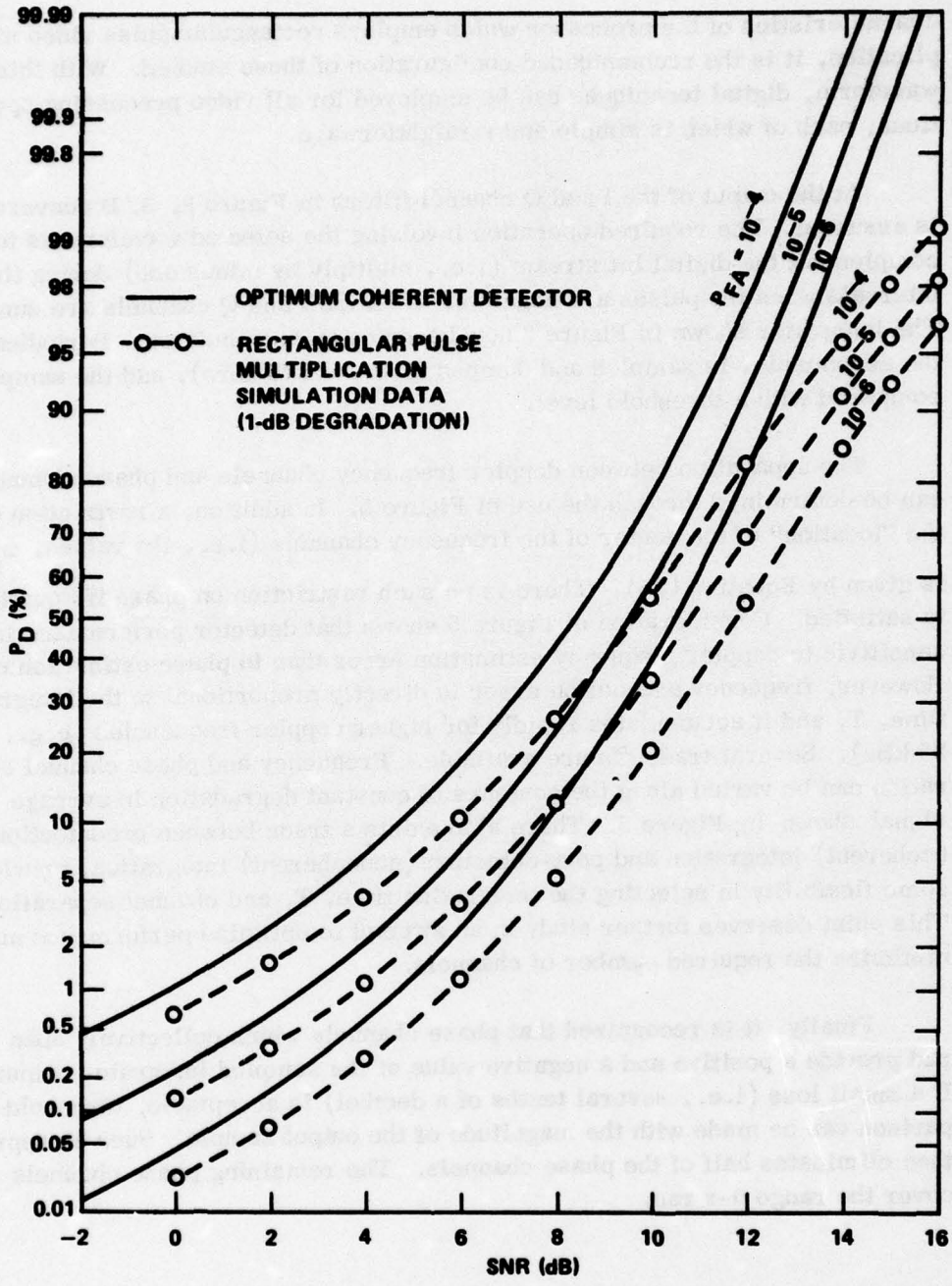

Figure 9. Probability of detection rectangular pulse multiplication.

characteristics of the processor which employs rectangular pulse video multiplication, it is the recommended configuration of those studied. With this waveform, digital techniques can be employed for all video processing operations, each of which is simple and straightforward.

At the output of the I and Q channel filters in Figure 2, A/D conversion is assumed. The required operation involving the selected waveform is to complement the digital bit stream (i.e., multiply by minus one) during time intervals when the pulses are negative. Next the I and Q channels are summed. The integrator shown in Figure 2 now becomes an accumulator. Periodically, the accumulator is sampled and dumped (i.e., set to zero), and the sample is compared with a threshold level.

The separation between doppler frequency channels and phase channels can be determined through the use of Figure 5. In addition, a restriction on the "location" of the center of the frequency channels (i.e., the values, ω_m) is given by Equation (26). There is no such restriction on phase if Equation (26) is satisfied. Consideration of Figure 5 shows that detector performance is less sensitivie to doppler frequency estimation error than to phase estimation error. However, frequency estimation error is directly proportional to the integration time, T, and it accumulates rapidly for higher doppler frequencies (e.g., 25 kHz). Several tradeoffs are available. Frequency and phase channel separation can be varied along the contours of constant degradation in average signal shown by Figure 5. There also exists a trade between predetection (coherent) integration and post-detection (noncoherent) integration, providing some flexibility in selecting the integration time, T, and channel separation. This point deserves further study in an attempt to optimize performance and minimize the required number of channels.

Finally, it is recognized that phase channels which collectively span 2π rad provide a positive and a negative value of the sampled integrator output. If a small loss (i.e., several tenths of a decibel) is acceptable, threshold comparison can be made with the magnitude of the output sample. Such an approach then eliminates half of the phase channels. The remaining phase channels cover the range $0-\pi$ rad.

V. SUMMARY AND RECOMMENDATIONS

This report presents the evolution of a video quasi-coherent detector having potential application to quiet radar. Results of particular interest are analyses and data pertinent to the comparative performance of the processing

schemes which employ sinusoidal and rectangular pulse train video multiplication. It is shown that the latter processor structure performs approximately 0.35 dB below the former in the presence and absence of doppler frequency and phase estimation errors. The performance of both processors is compared to that of an optimum coherent detector, which provides a performance benchmark. Design criteria are provided for separating the doppler frequency and the phase channels. The rectangular pulse processor configuration is recommended because it is conducive to the use of digital techniques which offer fast, compact, and relatively inexpensive computational capabilities.

Further study of the recommended processor configuration is necessary in several areas. These areas include investigation of the operation under out-of-range conditions, and determination of the tradeoffs available between predetection (coherent) integration, and post-detection (noncoherent) integration. Simulation programs developed during this reported work can be used to facilitate such future effort.

Appendix. DETECTOR PERFORMANCE FOR VARIOUS SIGNAL PROCESSOR CONFIGURATIONS AND THRESHOLD COMPARISON SCHEMES

Various video signal processing configurations and methods of making detection decisions by threshold comparison are considered in this appendix with the detector performance expressed as the probability of detection in each case. Curves and data are presented which depict detection probability as a function of S/N ratio for several values of detector false alarm probability. These results correspond to a single look, as post detection integration is not considered here.

For purposes of general usage in this appendix, the following expressions of signal plus noise are of interest:

$$x(T) = A \cos(\theta) + n_x(T) = u(T) + n_x(T) \tag{A-1}$$

$$y(T) = A \sin(\theta) + n_y(T) = v(T) + n_y(T) \tag{A-2}$$

where T is the time at which the integrator is sampled (Figure A-1). In Equations (A-1) and (A-2), A is a positive real constant, unless otherwise specified, and it is representative of the presence of a signal. The phase, θ, is a random variable which is uniformly distributed in the interval $-\pi$ to π rad. The terms $n_x(T)$ and $n_y(T)$ represent noise, and these are assumed to be independent gaussian random variables with zero mean value and variance, σ^2, taken from narrowband gaussian noise processes. Further, the constant A, the phase, and the noise components are assumed to be mutually independent. The probability density functions for the noise and signal components are, respectively, given by

$$f(n_x) = \frac{1}{\sigma\sqrt{2\pi}} \exp\ -n_x^2/2\sigma^2 \tag{A-3}$$

$$f(u) = \frac{1}{\pi\sqrt{A^2 - u^2}}\ , \quad -A \le u \le A \tag{A-4}$$

$$= 0, \text{ otherwise,}$$

with expressions of the same form for n_y and v.

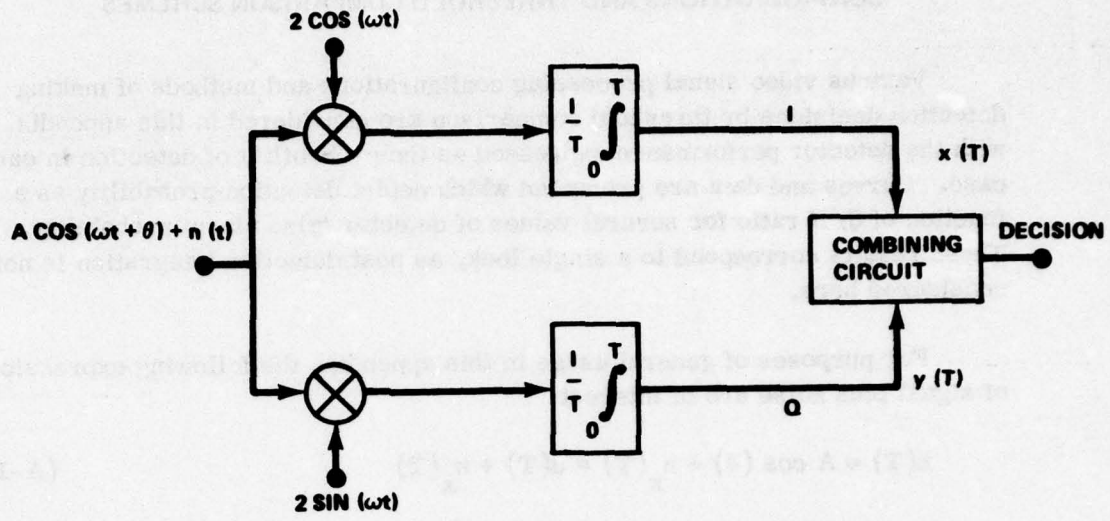

Figure A-1. I and Q channel video signal processor.

The expressions of Equations (A-1) and (A-2) represent sampled outputs of a signal processor such as shown in Figure A-1. These experssions are modified as necessary to fit the various cases considered in the following developments.

1. Case 1: A Coherent Signal Processor and Optimum Detection

In evaluating the performance of a detector, it is useful to compare its performance with that of the optimum detector under idealized conditions. For this reason, this case entails use of a coherent signal processor which requires that the received frequency and phase be exactly known. The sampled processor output then corresponds to Equation (A-1) with θ set equal to zero. In Figure A-1, this means that the signal is entirely in the I processor channel. Detection takes the form of comparison of the sampled outputs, x(T), with some threshold level which produces a desired probability of false alarm.

The probability density function for x(T) is

$$f(x) = \frac{1}{\sigma\sqrt{2\pi}} \exp\left[-(x - A)^2/2\sigma^2\right] \quad , \quad -\infty \leq x \leq \infty \qquad \text{(A-5)}$$

as shown in Figure A-2. To establish the threshold level, t_h, from a desired false alarm probability, P_F, the required relationship is

$$P_F = P(x > t_h) = \int_{t_h}^{\infty} f(x)\, dx \quad , \quad A = 0$$

$$= \frac{1}{2} \text{ erfc } \frac{t_h}{\sqrt{2}\sigma} \quad . \tag{A-6}$$

That is, false alarm probability is evaluated in the absence of signal. The previously mentioned complementary error function is a tabulated function, and it is defined as

$$\text{erfc}(t) = \frac{2}{\sqrt{\pi}} \int_{t}^{\infty} \exp(-r^2)\, dr \quad . \tag{A-7}$$

Values of threshold level can be obtained from Figure A-3, where the false alarm probability expression of Equation (A-6) is plotted as a function of the normalized threshold, t_h/σ.

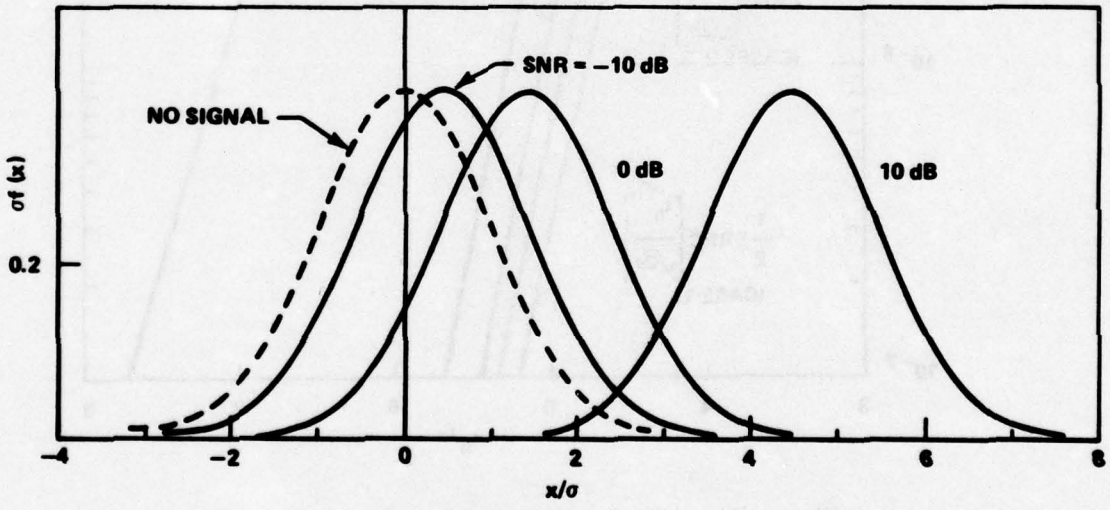

Figure A-2. Probability density function, Case 1.

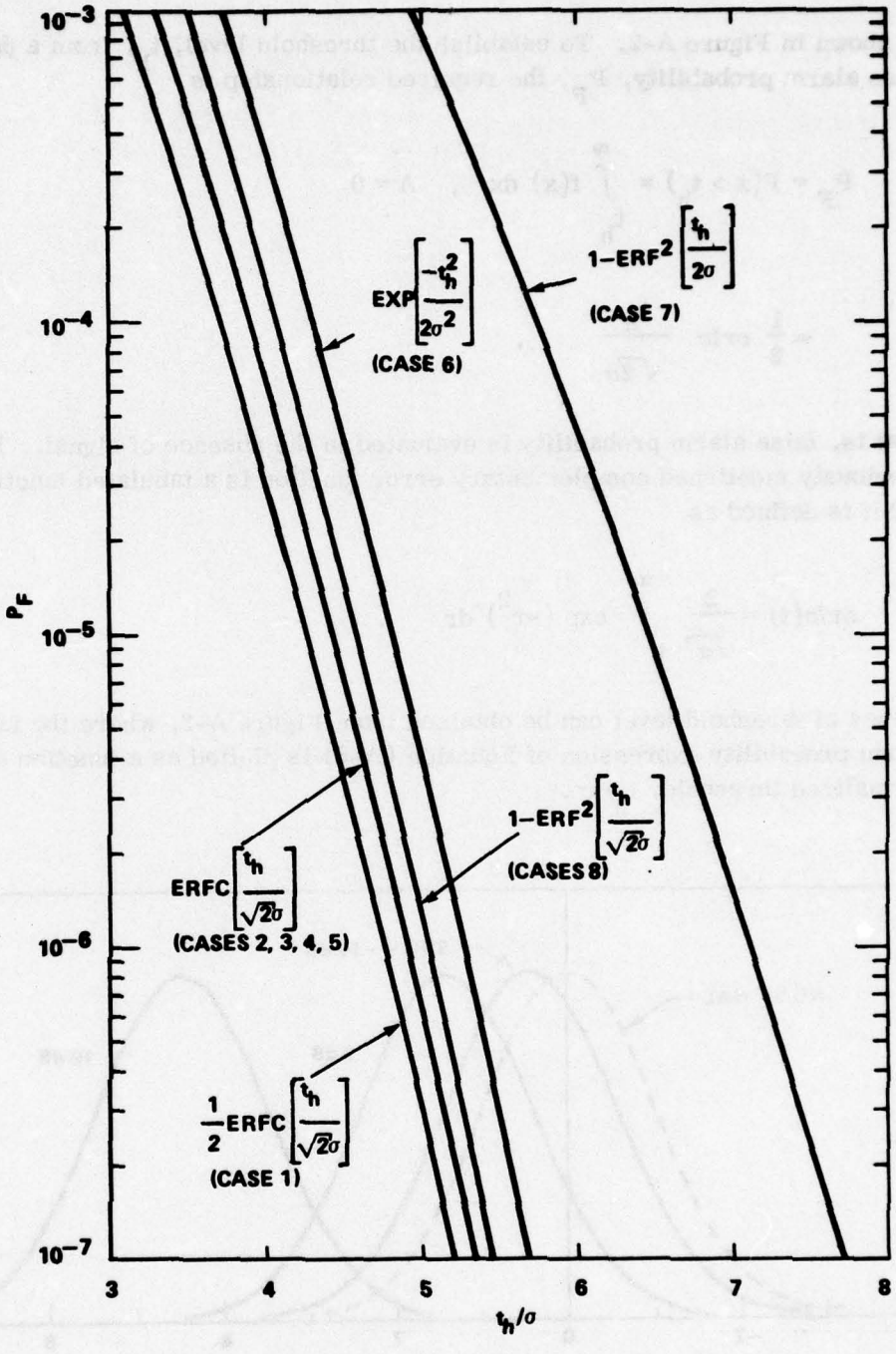

Figure A-3. Probability of false alarm, Cases 1-8.

With signal present, the probability of detection is expressed by

$$P_D = P(x > t_h) = \int_{t_h}^{\infty} f(x)\, dx$$

$$= \frac{1}{2} \operatorname{erfc}\left(\frac{t_h - A}{\sqrt{2}\sigma}\right) \quad . \tag{A-8}$$

For $A > t_h$, it is noted that

$$\operatorname{erfc}(-t) = 2 - \operatorname{erfc}(t) \quad , \quad t > 0 \quad . \tag{A-9}$$

The detection probability given by Equation (A-8) is shown in Figure A-4 as a function of

$$\text{SNR} = \frac{A^2}{2\sigma^2} \quad , \tag{A-10}$$

for several values of false alarm probability. In Equation (A-10), σ^2 is the variance of the noise out of each integrator in Figure A-1. For the general case, where θ is not zero, the SNR previously defined represents the S/N ratio following each integrator of Figure A-1, averaged over all values of θ. It also represents the S/N ratio of the coherent sum of the two channels, averaged over all θ. In any case, this ratio is dimensionally proper to define it as an S/N ratio.

2. Case 2: A Coherent Signal Processor with Magnitude Threshold Comparison

The signal processor in this case is that considered in the previous case. However, here detection decisions are based upon comparison of the magnitude of the sampled outputs of the processor with a threshold level. The probability density function of interest is that for

$$z(T) = |x(T)| \quad , \tag{A-11}$$

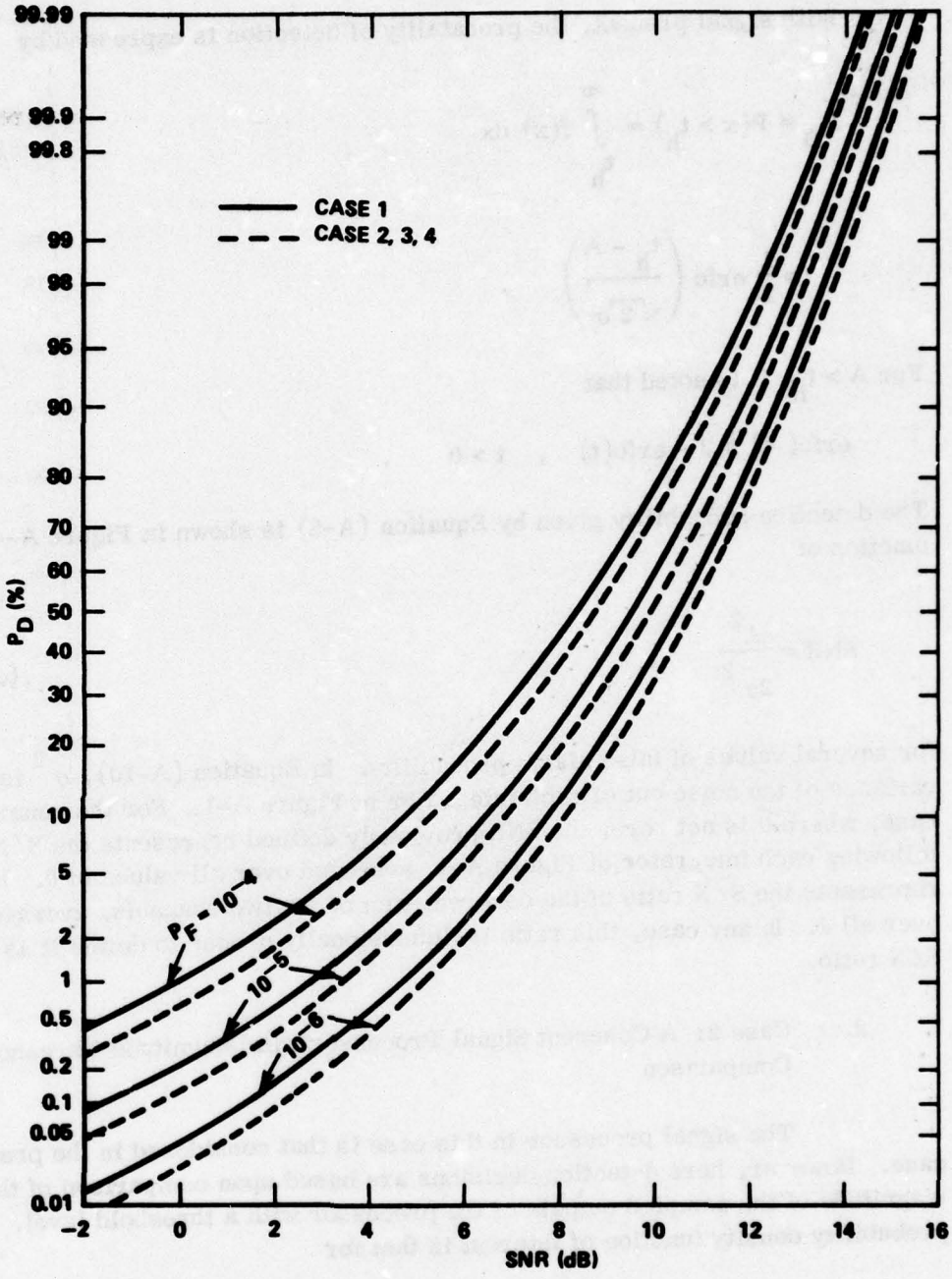

Figure A-4. Probability of detection, Cases 1-4.

where x(T) is given by Equation (A-1) with θ equal to zero. With the density function f(x) expressed by Equation (A-5), the probability density function corresponding to the magnitude of x(T) is

$$f_{|x|}(x) = \frac{1}{\sigma\sqrt{2\pi}} \{\exp[-(x-A)^2/2\sigma^2] + \exp[-(x+A)^2/2\sigma^2]\}\ ,$$

$$0 \leq x \leq \infty \qquad \text{(A-12)}$$

as shown in Figure A-5.

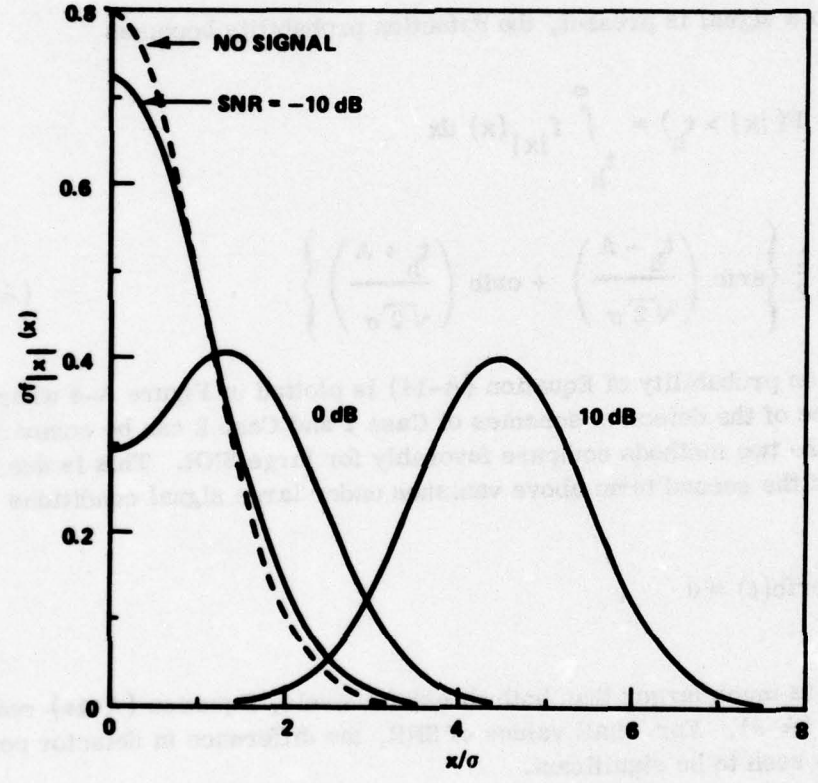

Figure A-5. Probability density function, Case 2.

In the absence of signal, the threshold level is related to the false alarm probability by

$$P_F = P(|x| > t_h) = \int_{t_h}^{\infty} f_{|x|}(x)\, dx = 2 \int_{t_h}^{\infty} f(x)\, dx \quad , \quad A = 0$$

$$= \text{erfc} \frac{t_h}{\sqrt{2}\sigma} \quad . \tag{A-13}$$

It is noted that the probability density function, $f(x)$, in the absence of signal is given by Equation (A-3). The previously mentioned false alarm probability is graphically shown in Figure A-3.

When a signal is present, the detection probability becomes

$$P_D = P(|x| > t_h) = \int_{t_h}^{\infty} f_{|x|}(x)\, dx$$

$$= \frac{1}{2} \left\{ \text{erfc} \left(\frac{t_h - A}{\sqrt{2}\sigma} \right) + \text{erfc} \left(\frac{t_h + A}{\sqrt{2}\sigma} \right) \right\} \quad . \tag{A-14}$$

The detection probability of Equation (A-14) is plotted in Figure A-4 where the performance of the detection schemes of Case 1 and Case 2 can be compared. As noted, the two methods compare favorably for large SNR. This is due to the fact that the second term above vanishes under large signal conditions since

$$\lim_{t \to \infty} \text{erfc}(t) = 0 \quad ,$$

and when A is much larger than both threshold levels, Equation (A-14) reduces to Equation (A-8). For small values of SNR, the difference in detector performance is seen to be significant.

3. Case 3: A Modified Coherent Signal Processor with Positive and Negative Threshold Comparison

In this case, the coherent processor of Case 1 is assumed to be modified such that it produces a 180° phase ambiguity in its estimation of the received signal phase. Thus, θ in Equation (A-1) is 0 or π rad with equal probability. Alternatively, θ can be set to zero while allowing A to take on positive and negative values with equal probability. Here, two thresholds, $\pm t_h$, are employed which are symmetrical about zero. The probability density function is[5]

$$f(x) = \frac{1}{\sigma 2\sqrt{2\pi}} \{\exp[-(x-A)^2/2\sigma^2] + \exp[-(x+A)^2/2\sigma^2]\} \quad . \quad \text{(A-15)}$$

In the absence of signal, the relationship between threshold level and false alarm probability is given by

$$P_F = P(x > t_h) + P(x < -t_h) = 2P(x > t_h)$$

$$= \frac{2}{\sigma\sqrt{2\pi}} \int_{t_h}^{\infty} \exp(-x^2/2\sigma^2)\, dx = \text{erfc}\left(\frac{t_h}{\sqrt{2}\sigma}\right) \quad . \quad \text{(A-16)}$$

The false alarm probability is graphically shown in Figure A-3, as it is the same function obtained previously in Equation (A-13).

The probability of detection in this case is given by the probabilities

$$P_D = P(x > t_h) + P(x < -t_h) \quad .$$

---

[5] The density function of Equation (A-15) is obtained by convolving the probability density function for the gaussian random variable with that for A. The latter density function is

$$f_A(u) = \frac{1}{2}\,\delta(u - A) + \frac{1}{2}\,\delta(u + A) \quad .$$

Due to the symmetry displayed by the probability density function, the two probabilities in the previously mentioned expression are equal. The detection probability can be written as

$$P_D = \int_{t_h}^{\infty} f(x)\,dx + \int_{-\infty}^{-t_h} f(x)\,dx = 2\int_{t_h}^{\infty} f(x)\,dx$$

$$= \frac{1}{2}\left\{\operatorname{erfc}\left(\frac{t_h - A}{\sqrt{2}\,\sigma}\right) + \operatorname{erfc}\left(\frac{t_h + A}{\sqrt{2}\,\sigma}\right)\right\} \quad , \qquad \text{(A-17)}$$

with f(x) expressed by Equation (A-15). Equation (A-17) is the same expression obtained for detection probability in Case 2, and given by Equation (A-14). Since the threshold levels are also related to false alarm by identical expressions, the two detectors perform in an equivalent manner.

4. Case 4: A Modified Coherent Signal Processor with Magnitude Threshold Comparison

Here, as in the previous case, it is assumed that the coherent processor is modified such that a 180° phase ambiguity in the estimation of the received signal phase results. The detection decision is based upon comparison of the magnitude of the sampled output with a threshold level. In the absence of signal, the situation is the same as that in Case 2. Thus, the probability of false alarm and threshold relationship is given by Equation (A-13).

The density function for x(T) is given by Equation (A-15), with signal present. Accounting for the magnitude of x(T), the probability density function becomes

$$f_{|x|}(x) = \frac{1}{\sigma\sqrt{2\pi}}\left\{\exp\left[-(x - A)^2/2\sigma^2\right] + \exp\left[-(x + A)^2/2\sigma^2\right]\right\} \quad ,$$

$$0 \le x \le \infty \quad . \qquad \text{(A-18)}$$

The detection probability is, therefore,

$$P_D = P(|x| > t_h) = \int_{t_h}^{\infty} f_{|x|}(x)\, dx$$

$$= \frac{1}{2}\left[\operatorname{erfc}\left(\frac{t_h - A}{\sqrt{2}\sigma}\right) + \operatorname{erfc}\left(\frac{t_h + A}{\sqrt{2}\sigma}\right)\right] \quad . \qquad \text{(A-19)}$$

This result too is the same as that obtained in Case 2 for the probability of detection. Thus, the two detection schemes are theoretically equivalent, and the detection probability is shown in Figure A-4 as a function of SNR.

5. Case 5: A Noncoherent Signal Processor with Magnitude Threshold Comparison

A noncoherent signal processor consisting of only the I channel in Figure A-1 is considered where the received signal has unknown phase in the presence of additive gaussian noise. The sampled output of the processor is described by Equation (A-1), where the parameter A is a positive real constant, θ represents a random variable uniformly distributed in the range $-\pi$ to π rad and $n_x(T)$ represents a zero mean gaussian random variable with variance, σ^2. With reference to Equation (A-1), the probability densities for $n_x(T)$ and $u(T)$ are given by Equations (A-3) and (A-4), respectively. Assuming independent phase and noise, the probability density function for $x(T)$ can be expressed in terms of the characteristic functions for the two densities.

Concerning $f(u)$, the characteristic function is

$$M_u(\xi) = \int_{-\infty}^{\infty} f(u) \exp(j\xi u)\, du = \frac{1}{\pi} \int_{-A}^{A} \frac{\exp(j\xi u)}{\sqrt{A^2 - u^2}}\, du \quad .$$

Making the variable change, $u = A\cos(\phi)$, the integral can be evaluated to produce

$$M_u(\xi) = J_0(A\xi) \quad , \qquad \text{(A-20)}$$

where $J_0(\cdot)$ is the zero order Bessel function of the first kind. Similarly, the characteristic function for the gaussian random variable with probability density f(n) is

$$M_n(\xi) = \frac{1}{\sigma\sqrt{2\pi}} \int_{-\infty}^{\infty} \exp(-n^2/2\sigma^2) \exp(j\xi n)\, dn$$

$$= \exp(-\xi^2\sigma^2/2) \quad . \tag{A-21}$$

In terms of the two characteristic functions, the density function for x(T) is given by

$$f(x) = \frac{1}{2\pi} \int_{-\infty}^{\infty} J_0(A\xi) \exp(-\xi^2\sigma^2/2) \exp(-j\xi x)\, d\xi \quad , \tag{A-22}$$

which is identified with the Fourier transform of the product of the characteristic functions. This integral cannot be evaluated in closed form. One method of obtaining numerical data representing this probability density is to utilize the fast Fourier transform algorithm (FFT).[6]

The detector addressed makes decisions based upon the magnitude of the processor output samples. Since both characteristic functions are even functions, the density function Equation (A-22) is real and even. Thus, the probability density for the magnitude of x(T) can be expressed in terms of Equation (A-22) as

---

[6] Note that Equation (A-22) must be expressed in the proper form when using the FFT to evaluate the integral. With the discrete Fourier transform (DFT) defined by

$$G(k) = \frac{T}{N} \sum_{m=0}^{N-1} g(m) \exp(-j2\pi km/N) \quad ,$$

Equation (A-22) must be rewritten using the variable change, $\beta = \sigma\xi/2\pi$. Here, T is the range of ξ over which the characteristic functions exist, and N is the number of sample points entered in an N-point FFT.

$$f_{|x|}(x) = 2f(x) \quad , \quad 0 \leq x \leq \infty \quad . \tag{A-23}$$

Illustrative densities are shown in Figure A-6 as obtained through the use of the FFT applied to Equation (A-22). Threshold is set to yield a desired false alarm probability according to

$$P_F = 2 \int_{t_h}^{\infty} f(x)\, dx \quad , \quad 0 \leq x \leq \infty \quad , \quad A = 0$$

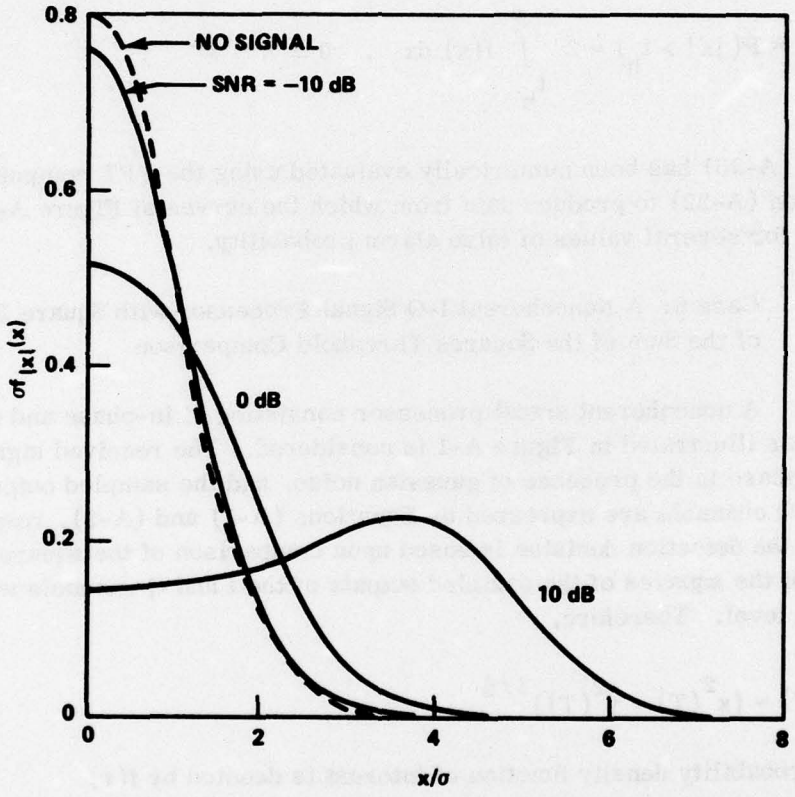

Figure A-6. Probability density function, Case 5.

where the probability density corresponds to the absence of signal. Under this condition, the false alarm probability is again

$$P_F = \frac{2}{\sigma\sqrt{2\pi}} \int_{t_h}^{\infty} \exp\left(-x^2/2\sigma^2\right) dx = \operatorname{erfc}\left(\frac{t_h}{\sqrt{2}\,\sigma}\right) \quad . \tag{A-24}$$

This probability appears graphically in Figure A-3 as a function of the normalized threshold, t_h/σ.

In the presence of signal, the probability of detection is obtained from Equation (A-23) to yield

$$P_D = P(|x| > t_h) = 2 \int_{t_h}^{\infty} f(x)\, dx \quad , \quad 0 \le x \le \infty \quad . \tag{A-25}$$

Equation (A-25) has been numerically evaluated using the FFT computations of Equation (A-22) to produce data from which the curves of Figure A-7 were prepared for several values of false alarm probability.

6. Case 6: A Noncoherent I-Q Signal Processor with Square Root of the Sum of the Squares Threshold Comparison

A noncoherent signal processor consisting of in-phase and quadrature channels as illustrated in Figure A-1 is considered. The received signal has unknown phase in the presence of gaussian noise, and the sampled outputs from the I and Q channels are expressed by Equations (A-1) and (A-2), respectively. Further, the detection decision is based upon comparison of the square root of the sum of the squares of the sampled outputs of the I and Q channels with a threshold level. Therefore,

$$r(T) = \left[x^2(T) + y^2(T)\right]^{1/2} \tag{A-26}$$

and the probability density function of interest is denoted by $f(r)$.

It is noted that the random variables which represent the signal components of Equations (A-1) and (A-2), $u(T)$ and $v(T)$, are not independent since they are related by θ. However, it is important to recognize that the

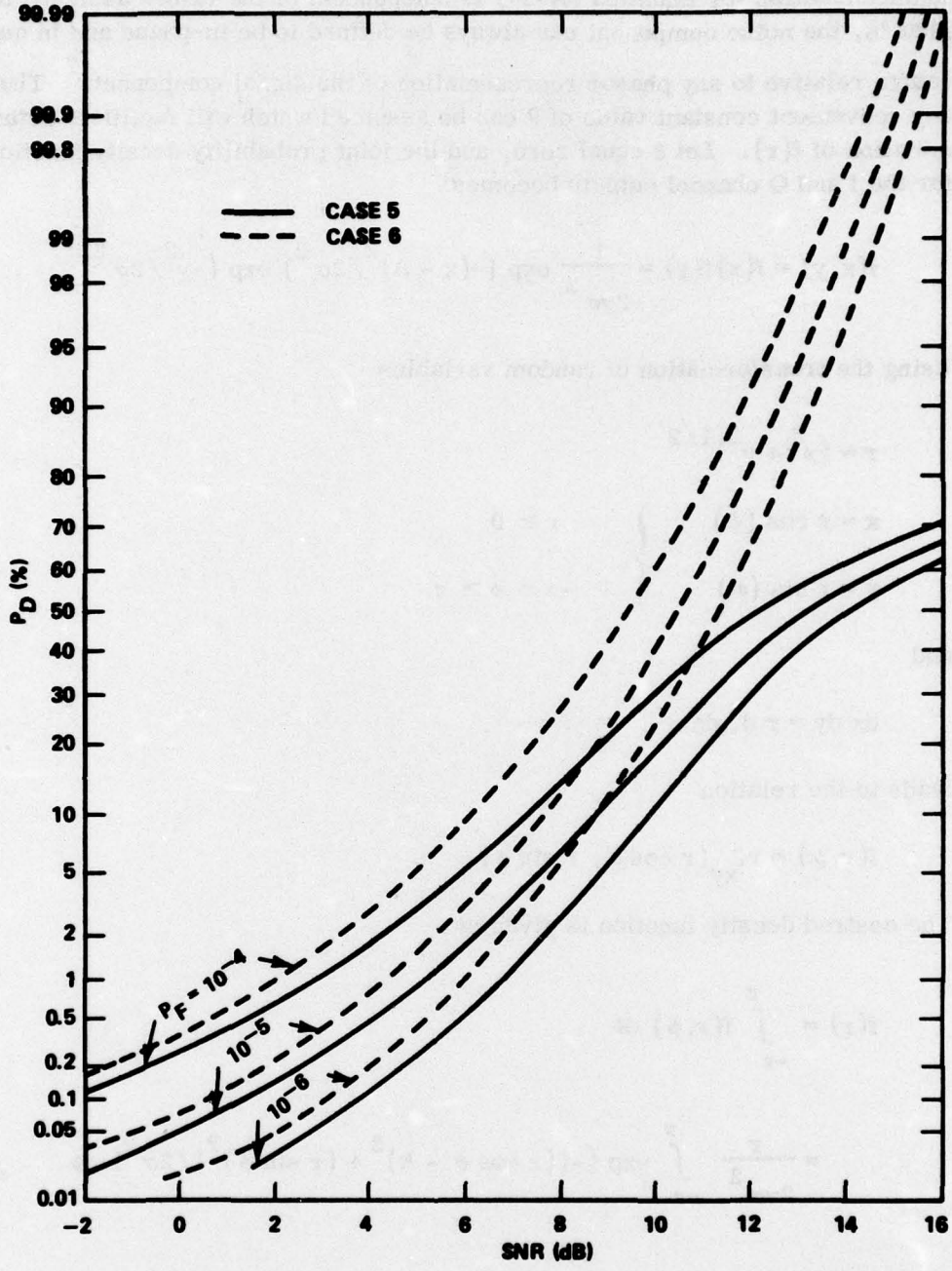

Figure A-7. Probability of detection, Cases 5 and 6.

density function for Equation (A-26) is independent of the values assigned to θ. That is, the noise component can always be defined to be in-phase and in quadrature relative to any phasor representation of the signal component.[7] Thus, any convenient constant value of θ can be assumed which will facilitate determination of f(r). Let θ equal zero, and the joint probability density function for the I and Q channel outputs becomes

$$f(x,y) = f(x)f(y) = \frac{1}{2\pi\sigma^2} \exp\left[-(x - A)^2/2\sigma^2\right] \exp\left(-y^2/2\sigma^2\right) \quad .$$

Using the transformation of random variables

$$\left.\begin{aligned} r &= (x^2 + y^2)^{1/2} \\ x &= r\cos(\phi) \\ y &= r\sin(\phi) \end{aligned}\right\} \qquad \begin{aligned} &r \geq 0 \\ &-\pi \leq \phi \geq \pi \end{aligned}$$

and

$$dx\,dy = r\,dr\,d\phi$$

leads to the relation

$$f(r,\phi) = r f_{xy}(r\cos\phi,\ r\sin\phi) \quad .$$

The desired density function is given by

$$f(r) = \int_{-\pi}^{\pi} f(r,\phi)\,d\phi$$

$$= \frac{r}{2\pi\sigma^2} \int_{-\pi}^{\pi} \exp\left\{-\left[(r\cos\phi - A)^2 + (r\sin\phi)^2\right]/2\sigma^2\right\} d\phi$$

---

[7] Beckmann, P., Probability in Communication Engineering, p. 122.

$$= \frac{r}{2\pi\sigma^2} \exp\left[-(r^2 + A^2)/2\sigma^2\right] \int_{-\pi}^{\pi} \exp\left[(rA\cos\phi)/\sigma^2\right] d\phi$$

$$= \frac{r}{\sigma^2} \exp\left[-(r^2 + A^2)/2\sigma^2\right] I_0\left(\frac{rA}{\sigma^2}\right) \quad , \qquad \text{(A-27)}$$

where $I_0(\cdot)$ is the zero order modified Bessel function. The Equation (A-27) is often referred to as the Rice-Nakagami density. As a matter of formality, the joint density function, $f(x,y)$ could be defined as a function of θ also. This would lead to a need to average over all θ in order to obtain $f(r)$. But with θ assumed uniformly distributed in the range $-\pi$ to π rad, the resultant would be Equation (A-27). The density function given by Equation (A-27) is graphically illustrated in Figure A-8.

The false alarm probability from which a threshold level is established is obtained from Equation (A-27) by setting A to zero. Under this condition, $I_0(0)$ has unit value, and the Rayleigh density function results. Thus,

$$P_F = P(r > t_h) = \int_{-t_h}^{\infty} f(r)\, dr \quad , \quad A = 0$$

$$= \exp\left(\frac{-t_h^2}{2\sigma^2}\right) \quad . \qquad \text{(A-28)}$$

This function is shown in Figure A-3, from which the normalized threshold level can be found for a given false alarm probability.

In the presence of signal, the probability of detection is expressed as

$$P_D = P(r > t_h) = \int_{t_h}^{\infty} f(r)\, dr \quad . \qquad \text{(A-29)}$$

This integral was numerically evaluated to obtain data from which the curves of Figure A-7 were constructed.

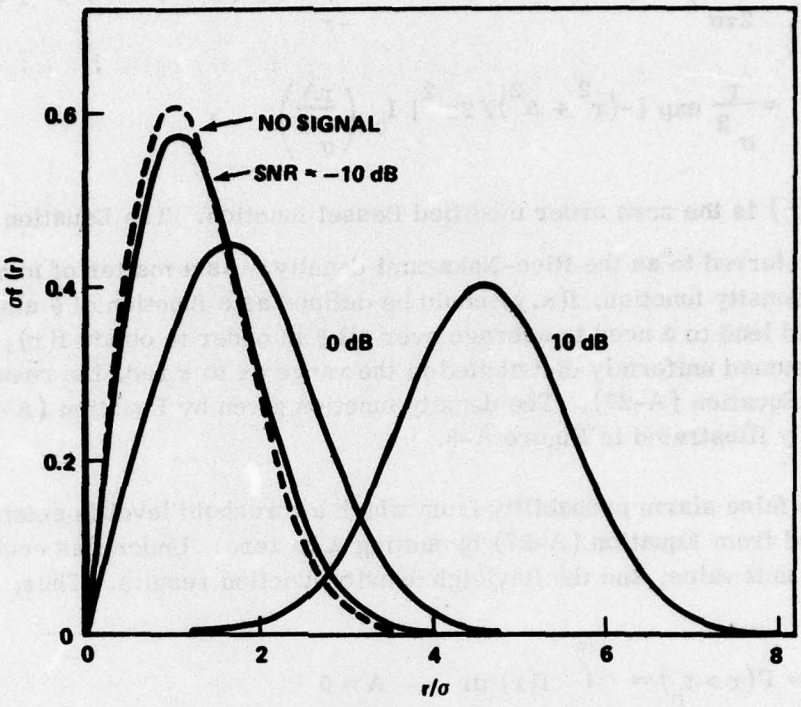

Figure A-8. Probability density function, Case 6.

In the foregoing development, it was asserted that the received signal phase could be assigned any value for purposes of finding the density function, f(r). This claim was substantiated during this effort by digital computer simulation of Equation (A-26), with x(T) and y(T) given by Equations (A-1) and (A-2). Several simulations were conducted. First, the phase, θ, was randomly selected in a uniform manner over the range of values, $-\pi$ to π rad, and the simulation was carried out. In addition, θ was assigned values of 10°, 30° and 40°, and three separate simulations were carried out. Each simulation conducted produced data for false alarm probabilities of 10^{-4}, 10^{-5}, and 10^{-6} as a function of SNR. Comparison of these data with the detection probability curves of Figure A-7 showed excellent agreement.

7. Case 7: A Noncoherent I-Q Signal Processor with the Sum of the Magnitudes Threshold Comparison

The I-Q signal processor of the previous case is again considered with detection decisions based upon comparison of the sum of the magnitudes of the sampled outputs from the I and Q channels

$$z(T) = |x(T)| + |y(T)| \tag{A-30}$$

with a threshold level. Again, $x(T)$ and $y(T)$ are expressed by Equations (A-1) and (A-2), with θ uniformly distributed in the range $-\pi$ to π rad. The density functions for the magnitudes of $x(T)$ and $y(T)$ are both of the form of Equation (A-22), but the two random variables are not independent.

In the absence of signal, the probability density function for $z(T)$ is obtained by convolving the magnitude gaussian noise density with itself, since the noise in the two channels is independent. The density function for each noise component has the form of Equation (A-3). Accounting for the magnitude of each gaussian random variable,

$$f(z) = \int_0^z f_{|N|}(n) f_{|N|}(z-n)\, dn$$

$$= \frac{4}{2\pi\sigma^2} \int_0^z \exp(-n^2/2\sigma^2) \exp[-(z-n)^2/2\sigma^2]\, dn$$

$$= \frac{2}{\sigma\sqrt{\pi}} \exp(-z^2/4\sigma^2)\, \mathrm{erf}(z/2\sigma) \quad , \quad 0 \le z \le \infty \quad . \tag{A-31}$$

Above, the error function is defined by

$$\mathrm{erf}(t) = \frac{2}{\sqrt{\pi}} \int_0^t \exp(-r^2)\, dr \quad . \tag{A-32}$$

The probability of false alarm is

$$P_F = P(z > t_h) = \int_{t_h}^{\infty} f(z)\, dz = 1 - \int_0^{t_h} f(z)\, dz \quad .$$

Substituting Equation (A-31) into the rightmost integral of the previously mentioned equation, and making the variable change, $r = z/2\sigma$, yields

$$P_F = 1 - \frac{4}{\sqrt{\pi}} \int_0^{t_h/2\sigma} \exp(-r^2)\, \mathrm{erf}(r)\, dr \quad .$$

This integral can be evaluated using the method of integration by parts in conjunction with the relation of Equation (A-32) between the two factors in the integrand. Carrying out these steps gives the false alarm probability

$$P_F = 1 - \mathrm{erf}^2\left(\frac{t_h}{2\sigma}\right) \quad . \tag{A-33}$$

The function given by Equation (A-33) is shown in Figure A-3 for purposes of determining a desired threshold normalized to σ.

Derivation of an expression for the detection probability requires that the density function for z(T) be known. Lacking such an expression, Equation (A-30) was simulated on the digital computer. The phase appearing in Equations (A-1) and (A-2) was randomly selected from a uniform distribution in the range of values, $-\pi$ to π rad. The I and Q noise samples were independently selected from two independent gaussian distributions. Results of the simulation appear in Figure A-9, which depicts detection probability. Each data point in the figure is the result of 300,000 simulated samples of z(T).

8. A Noncoherent I-Q Signal Processor with the Larger of the Magnitudes of I and Q Threshold Comparison

Once again, the I-Q channel processor of Case 6 is considered. Here, detection decisions are made by comparing the larger of the magnitude of the I and Q channel sampled outputs

$$z(T) = \mathrm{Max}\{\,|x(T)|\ ,\ |y(T)|\} \tag{A-34}$$

with a threshold level. The probability density functions for the magnitudes of x(T) and y(T) are both of the form of Equation (A-22); however, the random variables for the I and Q samples are not independent.

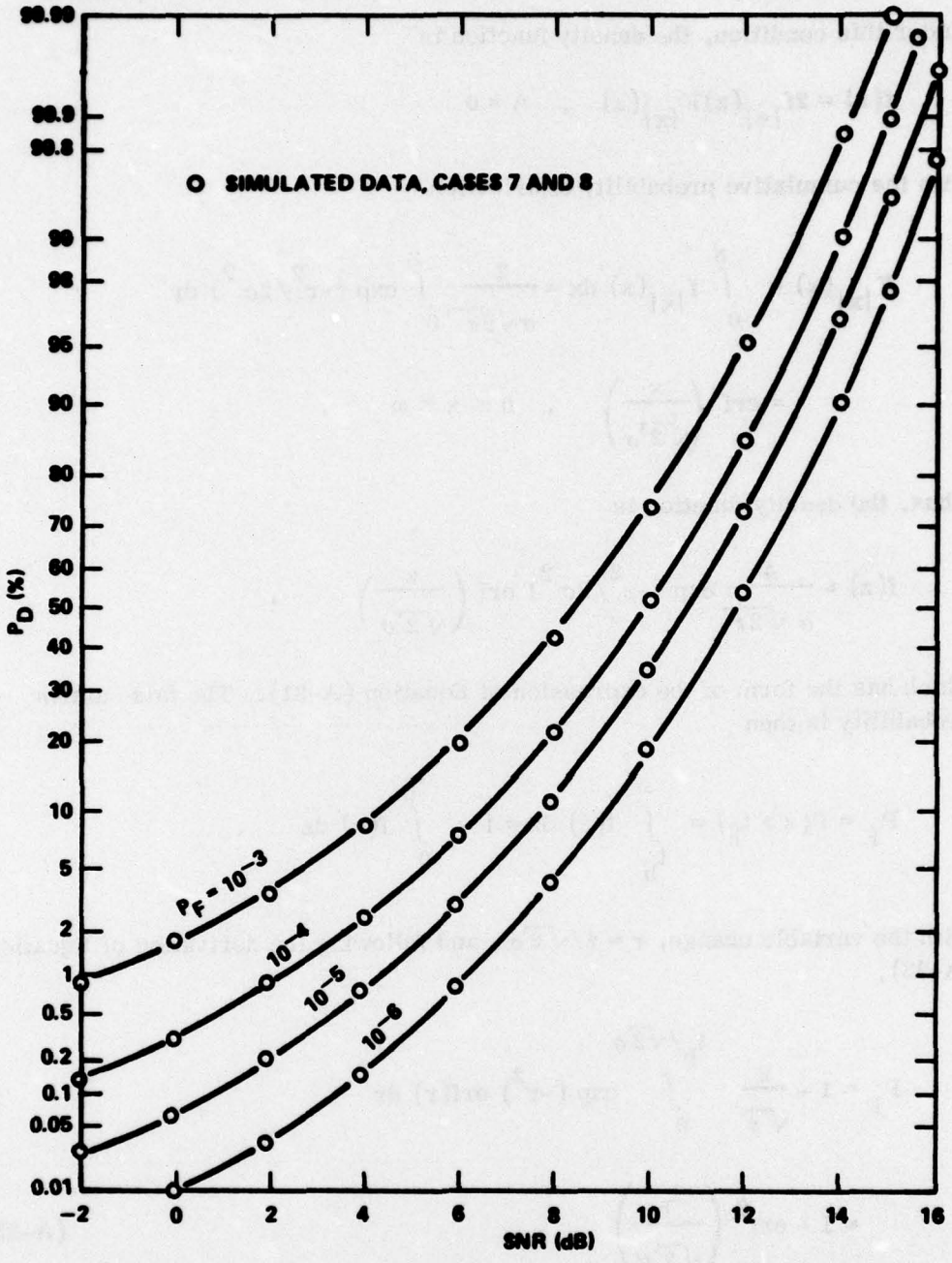

Figure A-9. Probability of detection, Cases 7 and 8.

In the absence of signal, the I and Q noise samples are independent. Under this condition, the density function is[8]

$$f(z) = 2f_{|x|}(z)F_{|x|}(z) \quad , \quad A = 0$$

with the cumulative probability distribution

$$F_{|x|}(x) = \int_0^x f_{|x|}(x)\, dx = \frac{2}{\sigma\sqrt{2\pi}} \int_0^x \exp\left(-r^2/2\sigma^2\right) dr$$

$$= \text{erf}\left(\frac{x}{\sqrt{2}\sigma}\right) \quad , \quad 0 \le x \le \infty \quad .$$

Thus, the density function is

$$f(z) = \frac{4}{\sigma\sqrt{2\pi}} \exp\left(-z^2/2\sigma^2\right) \text{erf}\left(\frac{z}{\sqrt{2}\sigma}\right) \quad ,$$

which has the form of the expression of Equation (A-31). The false alarm probability is then

$$P_F = P(z > t_h) = \int_{t_h}^{\infty} f(z)\, dz = 1 - \int_0^{t_h} f(z)\, dz \quad .$$

With the variable change, $r = z/\sqrt{2}\sigma$, and following the derivation of Equation (A-33),

$$P_F = 1 - \frac{2}{\sqrt{\pi}} \int_0^{t_h/\sqrt{2}\sigma} \exp\left(-r^2\right) \text{erf}(r)\, dr$$

$$= 1 - \text{erf}^2\left(\frac{t_h}{\sqrt{2}\sigma}\right) \quad . \qquad \text{(A-35)}$$

---

[8] Papoulis, A., Probability, Random Variables and Stochastic Processes, p. 193.

This function is shown in Figure A-3, from which values of normalized threshold levels can be obtained.

As in the previous case, the detection probability as a function of SNR for several values of false alarm probability was found by digital computer simulation. In this case, the resulting data values were found to be in complete agreement with those data obtained in Case 7. Thus, the detection schemes of Cases 7 and 8 are equivalent, a result stated by Nathanson.[9]

[9] Nathanson, F. E., Radar Design Principles, p. 474.

DISTRIBUTION

	No. of Copies
Defense Documentation Center Cameron Station Alexandria, Virginia 22314	12
Commander US Army Materiel Development and Readiness Command	
ATTN: DRCRD	1
DRCDL	1
5001 Eisenhower Avenue Alexandria, Virginia 22333	
DRSMI-FR, Mr. Strickland	1
-LP, Mr. Voigt	1
-R, Dr. McDaniel	1
Dr. Kobler	1
-RE	3
-REG	20
-RBD	3
-RPR (Record Set)	1
(Reference Copy)	1